



저작자표시 2.0 대한민국

이용자는 아래의 조건을 따르는 경우에 한하여 자유롭게

- 이 저작물을 복제, 배포, 전송, 전시, 공연 및 방송할 수 있습니다.
- 이차적 저작물을 작성할 수 있습니다.
- 이 저작물을 영리 목적으로 이용할 수 있습니다.

다음과 같은 조건을 따라야 합니다:

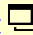


저작자표시. 귀하는 원저작자를 표시하여야 합니다.

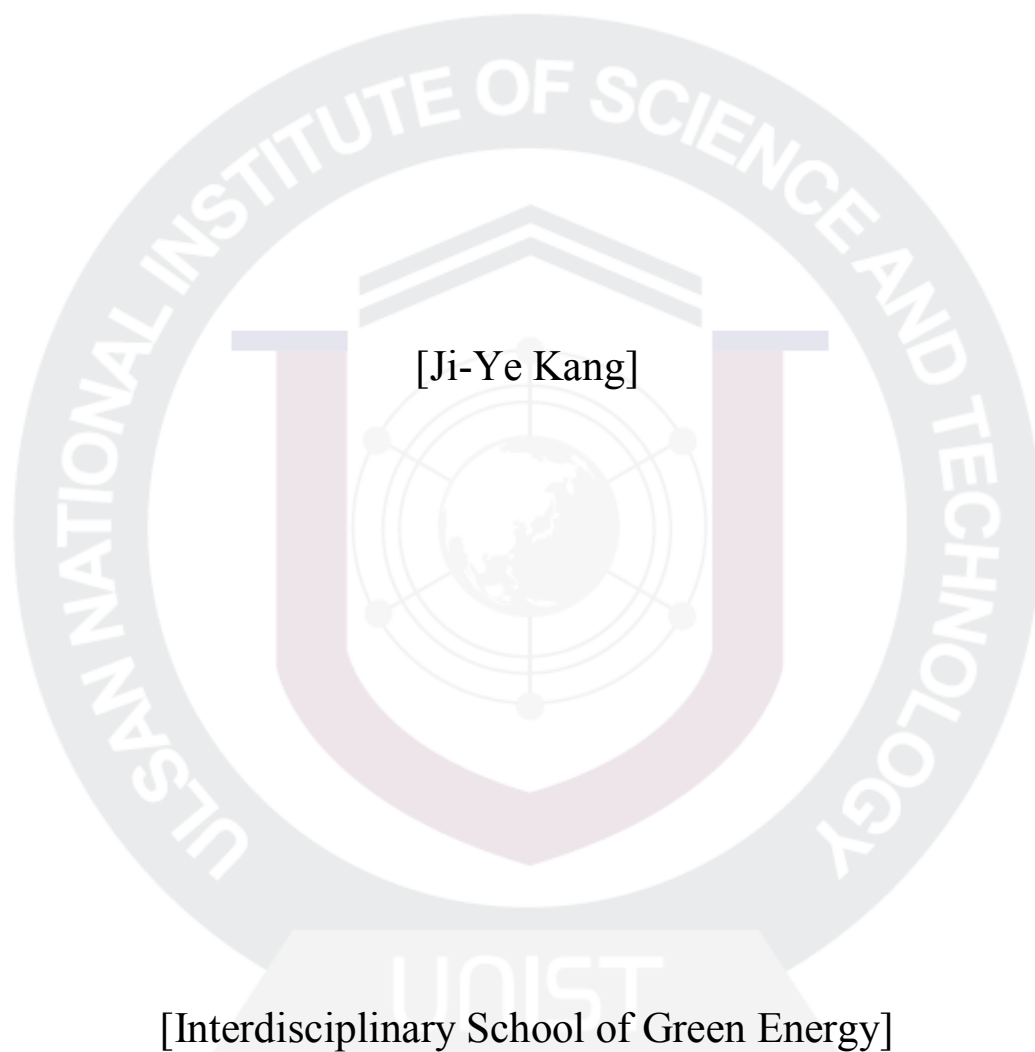
- 귀하는, 이 저작물의 재이용이나 배포의 경우, 이 저작물에 적용된 이용허락조건을 명확하게 나타내어야 합니다.
- 저작권자로부터 별도의 허가를 받으면 이러한 조건들은 적용되지 않습니다.

저작권법에 따른 이용자의 권리는 위의 내용에 의하여 영향을 받지 않습니다.

이것은 [이용허락규약\(Legal Code\)](#)을 이해하기 쉽게 요약한 것입니다.

[Disclaimer](#) 

**[Multifunctional poly(2,5-benzimidazole)/carbon
nanotube composite films]**



[Interdisciplinary School of Green Energy]

Graduate School of UNIST

[Multifunctional poly(2,5-benzimidazole)/carbon nanotube composite films]

A thesis
submitted to the Interdisciplinary School of Green Energy
and the Graduate School of UNIST
in partial fulfillment of the
requirements for the degree of
Master of Science.

[Ji-Ye Kang]

05. 28. 2010

Approved by

Major Advisor

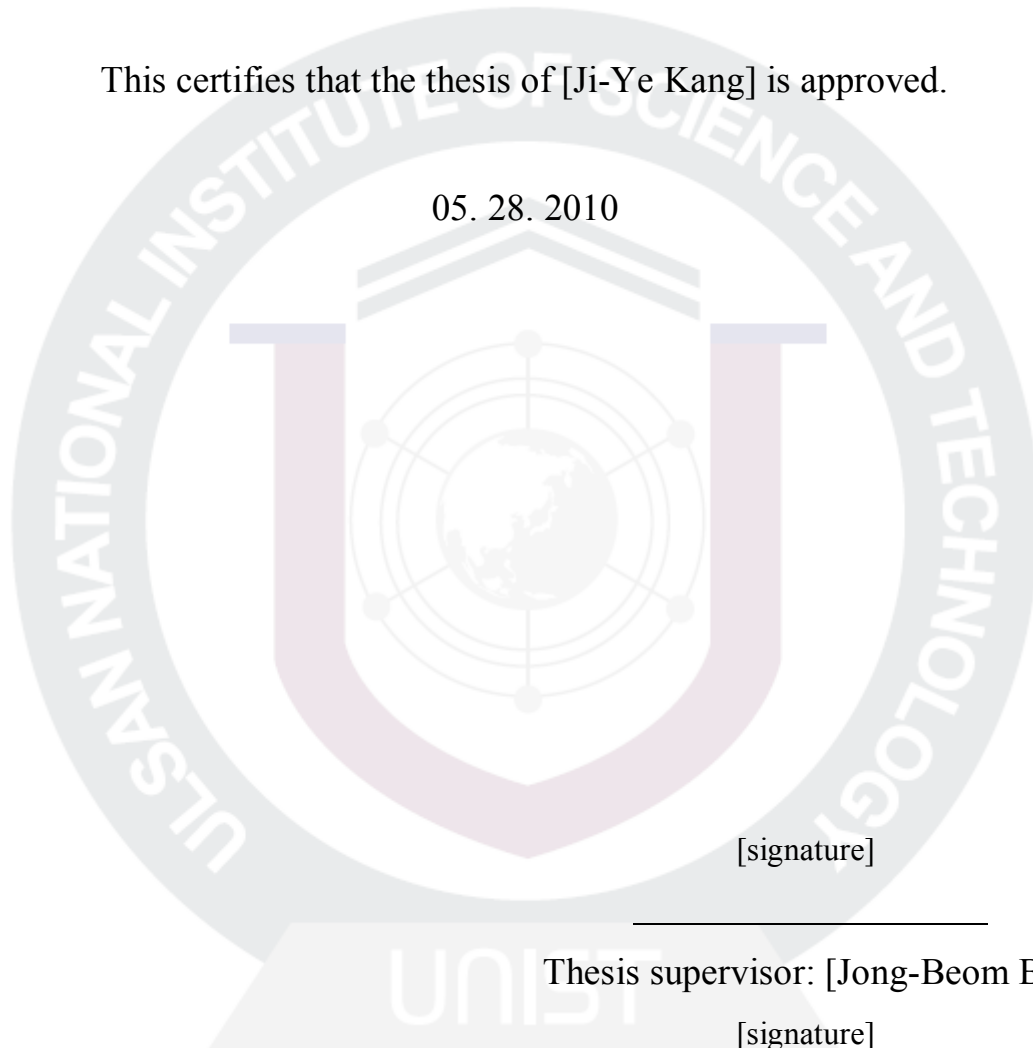
[Jong-Beom Baek]

[Multifunctional poly(2,5-benzimidazole)/carbon nanotube composite films]

[Ji-Ye Kang]

This certifies that the thesis of [Ji-Ye Kang] is approved.

05. 28. 2010



[signature]

Thesis supervisor: [Jong-Beom Baek]

[signature]

[Yongseok Jun]

[signature]

[Changduk Yang]

Abstract

The AB-monomer, 3,4-diaminobenzoic acid dihydrochloride, was recrystallized from an aqueous hydrochloric acid solution and used to synthesize high molecular weight poly(2,5-benzimidazole) (ABPBI). ABPBI/carbon nanotube (CNT) composites were prepared via *in-situ* polymerization of the AB-monomer in the presence of single-walled carbon nanotube (SWCNT) or multi-walled carbon nanotube (MWCNT) in a mildly acidic polyphosphoric acid (PPA). The morphology of these composite films was studied by x-ray diffraction and scanning electron microscopy. The results showed that both types of CNTs were uniformly dispersed into the ABPBI matrix. Tensile properties of the composite films were significantly improved as compared to ABPBI and their toughness (~200 MPa) was close to the nature's toughest spider silk (~215 MPa). The electrical conductivities of ABPBI/SWCNT and ABPBI/MWCNT composite films were 9.10×10^{-5} and 2.53×10^{-1} S/cm, respectively, while that of ABPBI film was 4.81×10^{-6} S/cm. Finally, without acid impregnation, while the ABPBI film was non-conducting, the SWCNT and MWCNT based composites were proton-conducting with maximum conductivities of 0.018 and 0.017 S/cm, respectively.

Contents

I . Introduction-----	1
II . Experimental-----	2
2.1 Materials-----	2
2.2 Instrumentations-----	3
2.3 Synthesis of Poly(2,5-benzimidazole) (ABPBI)-----	3
2.4 <i>In-situ</i> Polymerization of 3,4-Diaminobenzoic acid Hydrochloride with 10 wt% CNT Load-----	4
2.5 Film casting-----	4
III. Results and Discussion-----	5
3.1 <i>In-Situ</i> Polymerization-----	5
3.2 FT-IR Study-----	8
3.3 Thermal Properties-----	8
3.4 Scanning Electron Microscopy (SEM)-----	10
3.5 WAXS Patterns -----	12
3.6 UV-Absorption and Emission Spectra-----	13
3.7 Mechanical Properties -----	15
3.8 Electrical Conductivity of Films -----	16
3.9 Proton Conductivity of Films-----	17
IV. Conclusions-----	18
References-----	20
Appendix-----	25
Manuscript-----	32
Acknowledgement-----	33

List of figures

Figure 1. FTIR (KBr pellet) spectra: (a) SWCNT; (b) MWCNT; (c) ABPBI/SWCNT composite; (d) ABPBI/MWCNT composite; and (e) ABPBI.

Figure 2. TGA thermograms obtained with a heating rate of 10 °C/min after annealing samples at 300 °C for 10 min: (a) in air and (b) in nitrogen.

Figure 3. SEM images of samples: (a) the fracture surface of ABPBI film directly cast from reaction mixture ($\times 300$, scale bar is 20 μm); (b) the fractured surface of ABPBI film cast from MSA solution ($\times 10,000$, scale bar is 600 nm); (c) the fracture surface of ABPBI/SWCNT composite film directly cast from reaction mixture ($\times 33$, scale bar is 200 μm); (d) the fractured surface of ABPBI/SWCNT composite film cast from MSA solution ($\times 10,000$, scale bar is 600 nm); (e) the fracture surface of ABPBI/MWCNT composite film directly cast from reaction mixture ($\times 3000$, scale bar is 2 μm); and (f) the fractured surface of ABPBI/MWCNT composite film cast from MSA solution ($\times 10,000$, scale bar is 600 nm). The scale bar for the inset is 100 nm.

Figure 4. XRD patterns of samples: (a) ABPBI; (b) ABPBI/SWCNT; and (c) ABPBI/MWCNT.

Figure 5. (a) Digital photograph of sample solutions in MSA under 365 nm UV light; (b) UV-absorption spectra of samples in NMP with a drop of MSA; and (c) emission spectra of samples in NMP with a drop of MSA. Excitation wavelength was 415 nm: (i) ABPBI; (ii) ABPBI/SWCNT; (iii) ABPBI/MWCNT; (iv) SWCNT; and (v) MWCNT.

Figure 6. Representative stress–strain curves of samples, which were tested at 20 °C and relative humidity of 50%. The crosshead speed was 100% of gauge length per minute.

Figure 7. Proton conductivity of sample films, which was measured at relative humidity of 50%

List of tables

Table 1. Thermogravimetric (TGA) and Elemental Analysis (EA) Data

Table 2. XRD Analysis Data of Film Samples

Table 3. Tensile Properties and Electrical Conductivity of Film Samples



List of Schemes

Scheme 1. (a) Synthesis of poly(2,5-benzimidazole) (ABPBI) in polyphosphoric acid (PPA) at 175 °C; (b) in situ polymerization of 3,4-diaminobenzoic acid dihydrochloride as an AB monomer in the presence of single-walled carbon nanotube (SWCNT) or multi-walled carbon nanotube (MWCNT) to generate corresponding ABPBI/CNT composites.



Nomenclature

CNT	Carbon nanotube
SWCNT	Single-walled carbon nanotube
MWCNT	Multi-walled carbon nanotube
PPA	Polyphosphoric acid
P₂O₅	Phosphorous pentoxide
PBX	Polybenzazole
PBZT	Polybenzobisthiazole
PBO	Polybenzobisoxazole
PBI	Polybenzimidazole
ABPBO	Poly(2,5-or2,6-benzooxazole)
ABPBI	Poly(2,5-benzimidazole)
DABA	3,4-diaminobenzoic acid
HCl	Hydrochloric acid
MSA	Methanesulfonic acid
NMP	<i>N</i> -methyl-2-pyrrolidinone
FTIR	Fourier transform spectroscopy
TGA	Thermal gravimetric analysis
XRD	X-ray photoelectron spectroscopy
SEM	Scanning electron microscope
TEM	Transmission electron microscope

I . Introduction

Polymer-matrix composites have been studied for five decades as a special class of high-performance, light-weight materials that continue to play important roles in the current and emerging technologies for application areas ranging from structural, electronic, electromagnetic-shielding, to smart materials.¹ Typically, they are prepared by dispersing rigid and strong fibers such as glass and carbon fibers in a polymer matrix, and their resulting properties (primarily because of the surface area and aspect-ratio limitations associated with the reinforcement additive) are greatly dependent on the loading amount of a particular filler, which generally requires a significant quantity (~60 vol%).¹ On the other hand, nanoscale additives such as nanoclays,² nanoparticles,³ nanoplatelets⁴ and carbon nanotubes (CNTs)⁵ can overcome such limitations, and when dispersed in a polymer matrix, they could dramatically change the properties of resultant composite at lower loadings. Among them, CNTs such as single-walled carbon nanotubes (SWCNTs) and multi-walled carbon nanotube (MWCNTs) have attracted considerable attention due to expected excellent mechanical, thermal, electrical properties attributed to their unique structures that are also amenable to a wide range of chemical modification.⁶ They could be used as reinforcing additives, and thus deliver their outstanding properties to the supporting matrices.⁷ The resultant composites could be utilized in application areas, where affordable, lightweight, and multifunctional materials are required. To take advantage of their mechanical properties as predicted, several studies have been performed on CNTs and reported their reinforcement in various thermoplastics and thermoset matrices.⁸ However, there are two major obstacles for polymer/CNT composites to achieve maximum level of enhanced composite properties. First, it is nontrivial to achieve the effective aspect ratio by homogeneous dispersion of CNT in polymer matrix.⁹ This is followed by the necessity to (i) efficiently transfer the outstanding properties of CNT to the supporting matrix, and (ii) form effective percolation network at low loading. Hitherto, many efforts have been devoted to achieving homogeneous dispersion of CNTs in various matrix materials via physical methods aided by sonication,¹⁰ chemical methods using strong and oxidizing acids, such as sulfuric acid and nitric acid,^{6, 11} or procedures combined with applying sonication.¹² However, applying sonication often results in structural damages such as sidewall opening, breaking, and tubes being turning into amorphous carbon.¹³ Treatment in strong acids, specifically in nitric acid as a strong oxidizing agent, turns CNTs into CNT-oxides, which lose not only electrical conductivity but also structural integrity.¹⁴ Furthermore, even after achieving homogeneous dispersion, a strong interfacial adhesion between CNT and polymer matrix is required.¹⁵ A simple melt or solution mixing of polymer with CNT may not be efficient way for the homogeneous dispersion and effective wetting without chemically and/or physically chopping CNTs into shorter tubes. This results in reduced aspect ratio.¹⁶ Hence, controlled covalent grafting of

polymer onto the surface of CNT without or with minimal damage¹⁷ and/or *in-situ* polymerization of corresponding monomer in the presence of CNT are probably better routes to attaining strong interfacial interaction, and thus strengthening the reinforcement effect.¹⁸

We have developed one-pot purification and functionalization of carbon nanomaterials in a mild reaction medium comprising of polyphosphoric acid (PPA) with additional phosphorous pentoxide (P₂O₅).¹⁹ This has been proven to be a non-destructive reaction medium that does not damage CNT framework. It is also strong enough to promote efficient Friedel-Crafts-type polycondensation. Commercial grade PPA, which contains 83 wt% phosphorous pentoxide, has been optimized and used as a superior polymerization medium for the synthesis of high performance polybenzazoles (PBXs) such as rigid-rod polymers: polybenzobisthiazole (PBZT), polybenzobisoxazole (PBO), and polybenzobisimidazole (PBI), and rigid coil polymers: poly(2,5- or 2,6-benzooxazoles) (ABPBO) and poly(2,5-benzimidazole) (ABPBI).²⁰ Although a few PBX/CNT composites derived from *in-situ* polycondensation in PPA have been reported,²¹ the one-pot purification of SWCNT and preparation of composites via *in-situ* polymerization has not been reported. Furthermore, all previously reported approaches may incur structural damage of CNT framework by applying sonication and/or strong acid treatments. As a result, the electrical conductivity of PBX/CNT composites has not yet been optimized.^{10b}

Herein, we report an *in-situ* self-condensation of di-protonated AB-monomer, namely, 3,4-diaminobenzoic acid dihydrochloride, for the synthesis of ABPBI in the presence of SWCNT or MWCNT in an optimized PPA. The composite films were then evaluated for their thermal, mechanical, electrical and proton-conducting properties.

II. Experimental

2.1. Materials

All reagents and solvents were purchased from Aldrich Chemical Inc. or Tokyo Chemical Inc. and used as received, unless otherwise specified. The AB monomer, 3,4-diaminobenzoic acid, was recrystallized from 10 vol% (conc. HCl/H₂O, v/v) aqueous hydrochloric acid to give 3,4-diaminobenzoic acid dihydrochloride (HPLC purity > 99.99%, m.p. > 300 °C dec.). Both single-walled carbon nanotube (SWCNT, 30-40 wt% purity) and multi-walled carbon nanotube (MWCNT, CVD MWCNT 95 with diameter of ~20 nm and length of 10-50 μm) were obtained from Hanhwa Nanotech Co., LTD, Seoul, Korea.²²

2.2 Instrumentations

The melting points (m.p.) were determined on a Mel-Temp melting point apparatus and are uncorrected. Intrinsic viscosities were determined using Cannon-Ubbelohde No. 200 viscometer. Flow times were recorded for MSA solution and polymer concentrations were approximately 0.5-0.1 g/dL at 30.0 ± 0.1 °C. Fourier-transform infrared (FT-IR) spectra were recorded on a Jasco FT-IR 480 Plus spectrophotometer. Solid samples were imbedded in KBr disks. Elemental analyses were performed with a CE Instruments EA1110. Thermogravimetric analysis (TGA) was conducted in air and nitrogen atmospheres with heating rate of 10 °C/min using a Perkin-Elmer TGA7 thermogravimetric analyzer with TAC7 controller. UV-vis spectra were obtained from a Perkin-Elmer Lambda 35 UV/Vis spectrometer. Fluorescence studies were conducted with a Perkin-Elmer LS 55 fluorescence spectrometer. Applied excitation wavelength was UV absorption maximum of each sample. Wide-angle X-ray scattering (WAXS) patterns were recorded on Scintag DMS2000 diffractometer. The field emission scanning electron microscopy (FESEM) was done by using LEO 1530FE. The field emission transmission electron microscope (FETEM) was used a FEI Tecnai G2 F30 S-Twin. Proton conductivity was evaluated using a two-point probe method with a Solartron 1260 AC impedance analyzer with amplitude of 10 mV and a frequency range of 1 - 100,000 Hz at relative humidity of 50%. Each film sample was fixed in a Teflon conductivity test cell consisted of a working and a reference Pt electrodes. The sample conductivity was determined by using $\sigma = (1/R) \times (L/A)$, where R is the resistance, L is the sample thickness, and A is the cross-sectional area. Surface resistivity of films was measured with AIT CMT-SR1000N four-point probe. Average values were taken after twenty measurements from different locations. Tensile tests were carried out on a universal testing machine (Instron model-UTM, DY-TSM-10). The cross-head speed was 100% of gauge length per minute at 20 °C and 50% humidity. Average values of five out of seven tests were taken after the highest and lowest results were discarded. The images of atomic force microscope (AFM) were obtained from Veeco Multimode V. AFM samples were prepared by spin casting of polymer solution (a drop of MSA solution in 10 mL NMP) on silicon wafer. Energy minimized structures were performed by CS Chem 3D Std computational package (Version 8.0, Cambridge Soft Corporation, Cambridge, MA 02140).

2.3 Synthesis of Poly(2,5-benzimidazole) (ABPBI)

Into a 250 mL resin flask equipped with a high torque mechanical stirrer, nitrogen inlet and outlet, 3,4-diaminobenzoic acid dihydrochloride (5g, 22.2 mmol) and PPA (83% P₂O₅ assay; 50g) were placed and stirred under a dry nitrogen purge at room temperature for 24h to prevent drastic foaming caused by the release of hydrochloric acid gas. The color of heterogeneous mixture was red in the

beginning. After 6 hour, the color of opaque lump was changed to brown. When gas foaming was suppressed, the mixture was heated to 60 °C for additional 3h to ensure complete dehydrochlorination. During this period, the mixture became transparent and light green colored. Then, the temperature was increased stepwise to 100 and 150 °C for 6 and 24h, respectively. To ensure ring closure, the mixture was further heated to 175 °C for 3h. Visually, an increase in the viscosity of reaction mixture was noted as the polymerization proceeded. At the end of polymerization, the mixture was cooled to room temperature and distilled water was added. Big chunks of polymeric product were isolated and subjected to Soxhlet extraction. The product was extracted with water for three days to completely remove acidic reaction medium, and with methanol for three days to remove other low molar mass impurities, and finally freeze-dried under reduced pressure (0.5 mmHg) for 48h: $[\eta] = 5.23$ dL/g (MSA, 30 ± 0.1 °C). Anal. Calcd. for $C_7H_4N_2$: C, 72.40 %; H, 3.47 %; N, 24.12 %, O, 0%. Found: C, 58.43%; H, 4.38%; N, 18.66%; O, 15.29%. The electrical conductivity of solution cast film: $4.81 \times 10^{-6} \pm 8.6 \times 10^{-7}$ S/cm.

2.4 *In-situ* Polymerization of 3,4-Diaminobenzoic acid Hydrochloride with 10 wt% CNT Load

In the same set-up for ABPBI synthesis, 3,4-diaminobenzoic acid dihydrochloride (4.5 g), as-received SWCNT (0.5 g) or MWCNT (0.5 g), and PPA (50 g) were placed. The rest of reaction sequence and work-up procedure were the same as the synthesis of ABPBI homopolymer. The initial color of all reaction mixtures was black because of the SWCNT or MWCNT dispersion. At the end of the polymerization, the color of the mixture was dark shiny brown, and the mixture was poured into distilled water to form a long single filament. The resulting fibrous bundles were worked up following the same procedure for ABPBI homopolymer.

ABPBI/SWCNT composite: $[\eta] = 6.61$ dL/g (MSA, 30 ± 0.1 °C). Anal. Calcd. for $C_{8.08}H_4N_2$: C, 77.29%; H, 2.86%; N, 19.85%; O, 0%. Found: C, 59.23%; H, 3.48%; N, 15.72%; O, 12.27%. The electrical conductivity of solution cast film: $9.10 \times 10^{-5} \pm 8 \times 10^{-6}$ S/cm.

ABPBI/MWCNT composite: $[\eta] = 5.31$ dL/g (MSA, 30 ± 0.1 °C). Anal. Calcd. for $C_{8.08}H_4N_2$: C, 77.29%; H, 2.86%; N, 19.85%; O, 0%. Found: C, 64.73 %; H, 3.75 %; N, 16.29 %; O, 12.58%. The electrical conductivity of solution cast film: $2.53 \times 10^{-1} \pm 0.01$ S/cm.

2.5 Film casting

Films were cast from each composite sample (1.0 g) dissolved in methanesulfonic acid (MSA, 20 mL). The resultant homogeneous solutions were cast onto leveled glass plate in a custom-made film casting apparatus. MSA was slowly removed by heating the apparatus to 80 °C under reduced

pressure (0.5 mmHg). The resultant uniform films were removed from glass plate after immersion in distilled water. They were sandwiched between Teflon membranes to them flat, and then kept under distilled water for 4 days. The films were further Soxhlet-extracted with water for three days and methanol for additional three days to ensure complete removal of residual MSA. FT-IR spectra of the films showed there was no trace of residual MSA. The films were cut into size for property evaluation.

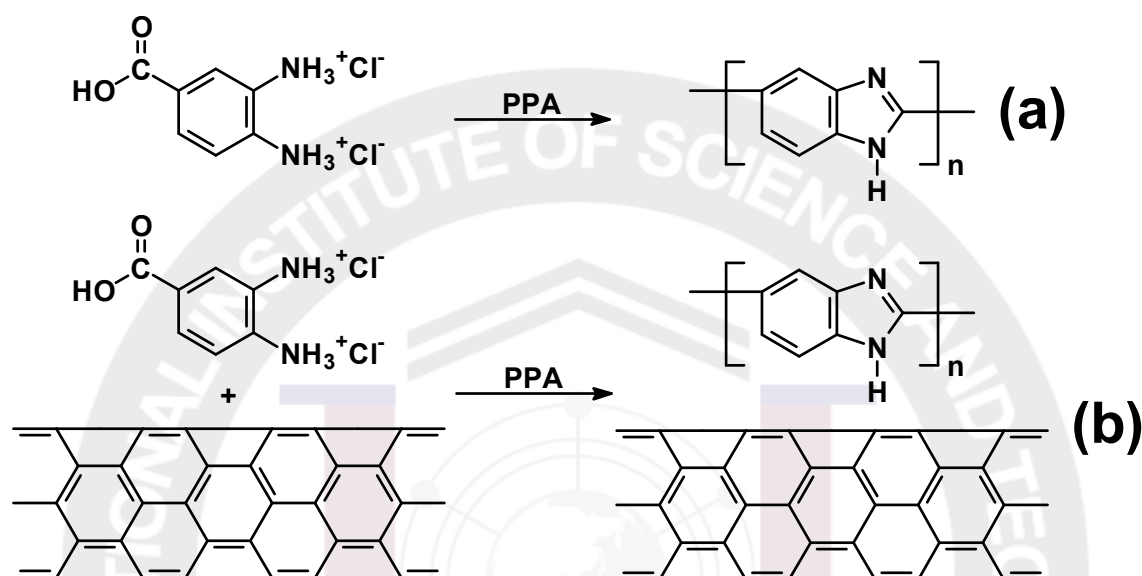
III. Results and Discussion

Amongst PBXs, PBIs are known for their outstanding thermal stability, mechanical and electrical properties, and chemical resistance.²³ They are currently used as thermal insulating materials and have potential applications as high strength fibers,²⁴ gas-separation and fuel-cell membranes.²⁵ Yet, in spite of extensive work in rigid-rod PBI, there are few reports on rigid-coil ABPBI.²⁶ Among the PBI family, ABPBI has the simplest structure and can be easily prepared from a single, inexpensive, and commercially available AB-monomer, i.e. 3,4-diaminobenzoic acid (DABA), via polycondensation in PPA. Hence, it has recently attracted much attention as an emerging material for high temperature fuel cell membrane to replace the expensive and electrochemically less stable Nafion family.²⁵

3.1 *In-Situ* Polymerization

The synthesis of poly(2,5-benzimidazole), which is also known as ABPBI, has been reported in early 1960's.^{23b,27} However, the molecular weights of ABPBI, when it is prepared from as-received AB monomer, namely 3,4-diaminobenzoic acid available from several commercial sources with purity 95-97%, are relatively low with inherent viscosity (1.4 - 2.7 dL/g) in concentrated sulfuric acid at 30 °C.^{25,28} It is also known that polymerization of rigorously purified 3,4-diaminobenzoic acid in either phosphoric acid/P₂O₅²⁹ or methanesulfonic acid/P₂O₅³⁰ mixtures has led to high molecular weight ABPBI. In this study, commercial 3,4-diaminobenzoic acid was recrystallized from an aqueous hydrochloric acid solution (water/concentrated hydrochloric acid, 90/10, v/v) to yield highly pure 3,4-diaminobenzoic acid dihydrochloride (purity > 99.99+%, HPLC). In fully protonated form, it is expected that 3,4-diaminobenzoic acid would have longer shelf-life than in acid-free form. In addition, we surmise that hydrochloric acid, which can be *in-situ* generated at room temperature during the slow dehydrochlorination of dihydrochloride monomer, could raise the acidity of the reaction medium that might improve both the dispersion and purification of CNTs by optimized PPA. Specifically, as-prepared SWCNT contains various impurities such as metallic particles, carbonaceous impurities, and amorphous carbons. The acidity of gaseous hydrochloric acid (pK_a ~ -8) is many orders of magnitude stronger than PPA (pK_a of H₃PO₄ or orthophosphoric acid ~ 2) and thus, the

population of protonated on the surface of CNT under such conditions should be higher, making the solvation of CNT in PPA more effective.³¹ After dehydrochlorination is completed by stepwise heating from room temperature to 150 °C in PPA, the reaction mixture is further heated to 175 °C for 3h to ensure complete imidazole ring closure, resulting in high molecular-weight ABPBI (Scheme 1a).³²



Scheme 1. (a) Synthesis of poly(2,5-benzimidazole) (ABPBI) in polyphosphoric acid (PPA) at 175 °C; (b) in situ polymerization of 3,4-diaminobenzoic acid dihydrochloride as an AB monomer in the presence of single-walled carbon nanotube (SWCNT) or multiwalled carbon nanotube (MWCNT) to generate corresponding ABPBI/CNT composites.

For the concurrent dispersion and purification of CNT in PPA, and the polymerization of the AB monomer in one-pot process to generate *in-situ* ABPBI/CNT composites, the polycondensation of the 3,4-diaminobenzoic acid dihydrochloride was carried out in the presence (10 wt% based on the monomer feed) of SWCNT or MWCNT (Scheme 1b). The initial color of all reaction mixtures was black because of the SWCNT or MWCNT dispersion. The color then became dark, shiny brown as polymerization progressed, which was taken as an indication for the homogeneous dispersion of CNTs. In both cases, the reaction mixtures were homogeneous with drastic increase in viscosity, when reaction temperature was approaching 150 °C. However, the solution behaviors of final reaction mixtures were clearly different between ABPBI and ABPBI/CNT composites. The ABPBI mixture at 175 °C was too viscoelastic to have efficient flow, and it was difficult to spin a fiber by simply pouring its hot polymerization dope into distilled water. On the other hand, both CNT-containing reaction mixtures at the similar temperature flowed quite well to yield long fibers upon similar workup. All isolated products were then Soxhlet-extracted with water for 3 days to ensure the

complete removal of residual PPA. They were further Soxhlet extracted with methanol for 3 days for the removal of other low molar mass impurities and then freeze-dried. The intrinsic viscosity of resultant ABPBI was ~ 5.23 dL/g (MSA, 30 ± 0.1 °C), which is higher than literature values (1.4-2.7 dL/g in 96% sulfuric acid at 30 °C).²⁵ The intrinsic viscosities of ABPBI/SWCNT and ABPBI/MWCNT composites were 6.61 and 5.31 dL/g (MSA, 30 ± 0.1 °C), respectively, and these values are higher than that of ABPBI. It is important to point out that the dilute solutions, in terms of reduced and inherent viscosities, of both ABPBI/SWCNT and ABPBI/MWCNT composites have behaved very similar to that of ABPBI. This comparison not only implicates that the polycondensation of the AB-monomer was not affected by the presence of CNTs, but also a strong polymer-CNT interaction (i.e. polymer wrapping) exists for these composites.

In all cases, final yields were higher than maximum calculated yields even after complete work-up procedures. This discrepancy might be related to the hygroscopic nature of ABPBI. Likewise, the large discrepancy between theoretical and experimental CHN contents in elemental analysis (Table 1) should also be attributed to bounded water in. ABPBI/SWCNT composite showed relatively larger discrepancy of C content and it was presumably due to the low carbon content of as-received SWCNT (see Table 1).

Table 1. Thermogravimetric (TGA) and Elemental Analysis (EA) Data

Sample	TGA ^a				Elemental Analysis			
	In Air		In N ₂		C	H	N	
	T _{d5%} (°C)	Char 800 °C (%)	T _{d5%} (°C)	Char 800 °C (%)	(%)	(%)	(%)	
ABPBI	611	42.3	656	86	Calcd	72.40	3.47	24.12
					Found	57.01	4.58	19.07
SWCNT	371	57	623	71.0	Calcd	100.00	0.00	0.00
					Found	82.84	0.74	- ^b
MWCNT	574	~0	789	94.6	Calcd	100.00	0.00	0.00
					Found	97.81	0.30	- ^b
ABPBI/SWCNT	578	11.2	658	88	Calcd	77.29	2.86	19.85
					Found	61.56	3.86	16.88
ABPBI/MWCNT	607	26.6	668	88	Calcd	77.29	2.86	19.85
					Found	64.80	3.84	15.87

^a The temperature at which 5% weight loss (T_{d5%}) occurred on TGA thermogram obtained with heating rate of 10 °C/min.

^b Below detection limit.

3.2 FT-IR Study

The transmittance of CNT samples was very poor due to the fact that CNTs strongly absorb infrared light (Figure 1a and 2b). They did not show comparable peaks at the same degree of magnification, while ABPBI, ABPBI/SWCNT and ABPBI/MWCNT displayed a strong and broad (OH) around 3500 cm^{-1} , which is attributed largely to the bounded water in hygroscopic ABPBI. There are characteristic C=N and C-N stretching bands at 1628 and 1287 cm^{-1} , respectively (Figure 1), which are assignable to the imidazole moiety of ABPBI polymer. The peaks from 3500 to 3300 cm^{-1} were attributed to the isolated N-H stretch of the imidazole ring, whereas the broad band near 3300 - 3150 cm^{-1} is due to intermolecular hydrogen-bonded $\text{H}\cdots\text{N}\cdots\text{H}$ structures, and it becomes broader in the presence of moisture. The only difference between ABPBI and ABPBI/CNT composites was the relative intensity of respective peaks. There were no discernable characteristic peaks among samples (Figure 1).

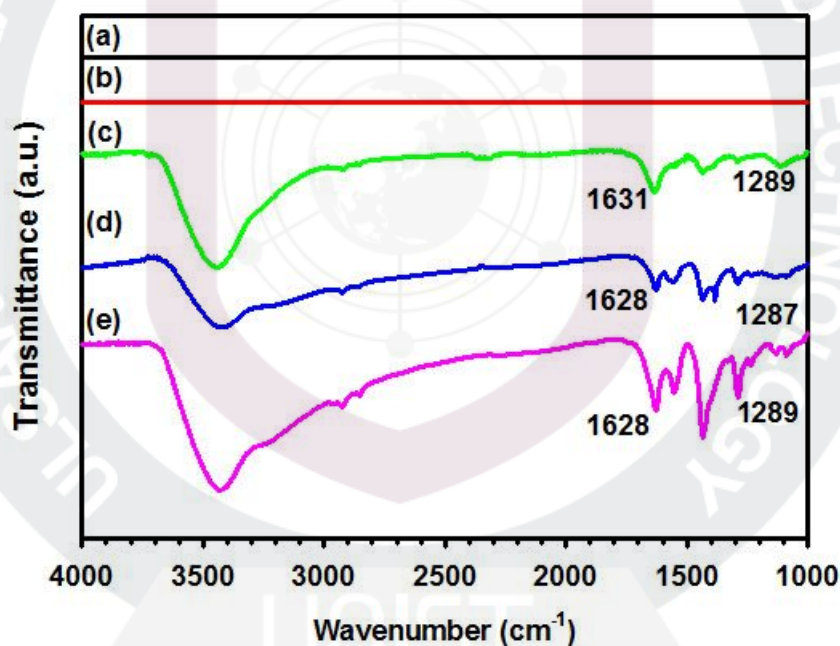


Figure 1. FTIR (KBr pellet) spectra: (a) SWCNT; (b) MWCNT; (c) ABPBI/SWCNT composite; (d) ABPBI/MWCNT composite; and (e) ABPBI.

3.3 Thermal Properties

The thermograms obtained from differential scanning calorimetry (DSC) characterization are not included because ABPBI has expectedly its transition temperature higher than its degradation temperature.^{23b} In all cases, the thermograms showed featureless traces, except for a broad

endothermic peak around 150 °C, which is caused by the release of polymer-bounded water from the sample.

To minimize effect from the contribution of bounded water, all samples were annealed in the chamber of thermogravimetric analyzer (TGA) at 300 °C for 10 min prior to analysis. After cooled down to room temperature, the samples were heated to 800 °C with the ramping rate of 10 °C/min for experiments conducted in both air and nitrogen. The ABPBI, SWCNT, MWCNT, ABPBI/SWCNT, and ABPBI/MWCNT samples showed that the temperature at which 5% weight loss ($T_{d5\%}$) in air occurred at 574, 371, 611, 607, and 578 °C, in that order (Figure 2a and Table 1). Among these samples, SWCNT started to decompose at the lowest temperature, presumably because of the thermo-oxidative instability (combustion) of amorphous carbon. It should be noted that the char yield of as-received SWCNT at 800 °C was 57%, while that of MWCNT was practically 0%. The high-residue yield of SWCNT at 800 °C in air is most probably due to more combustion-resistant impurities, such as metallic catalyst particles and crystalline carbonaceous impurities.³³ Surprisingly, ABPBI homopolymer displayed the highest thermo-oxidative stability among the samples in air ($T_{d5\%}=611$ °C), which is 240 °C and 37 °C higher than those of as-received SWCNT ($T_{d5\%}=371$ °C) and MWCNT ($T_{d5\%}=574$ °C), respectively. In contrast to the expectation, ABPBI turned out to be the component that had improved thermo-oxidative stability of the ABPBI/CNT composites. The comparison of char yields at 800 °C in air could be considered as a qualitative assessment of SWCNT purity. Taking into account of the loaded SWCNT amount (10 wt%), ABPBI/SWCNT was expected to display higher char yield (11.2%) at 800 °C than those of ABPBI (42.3%) and ABPBI/MWCNT (26.6%). However, the amount of residues was the lowest among them, implying that the tenacious (and thermo-oxidatively stable) impurities present in as-received SWCNT were almost all removed during the polymerization and work-up stages. This rationalization implicated that a mildly acidic PPA medium with additional hydrochloric acid, which was *in-situ* generated from AB monomer, might be an efficient way for the purification of as-received SWCNT.^{19c}

Under nitrogen atmosphere, as-received MWCNT apparently was the most stable with $T_{d5\%}$ at 789 °C and char yield at 800 °C was 94.6 wt% (Figure 2b). Unlike in air atmosphere, as-received SWCNT displayed better thermal stability in nitrogen. It had $T_{d5\%}$ at 623 °C and its char yield at 800 °C was 71.0 wt%. The $T_{d5\%}$ of ABPBI, ABPBI/SWCNT, and ABPBI/MWCNT at 800 °C was similar at 656, 658, and 668 °C, corresponding to char yield of 86, 88 and 88 wt%, respectively.

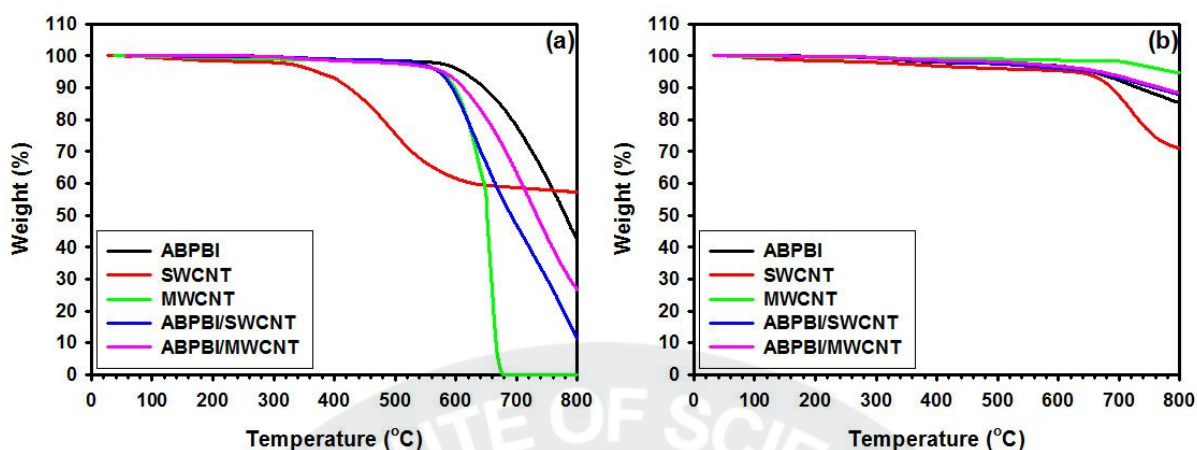


Figure 2. TGA thermograms obtained with a heating rate of 10 °C/min after annealing samples at 300 °C for 10 min: (a) in air and (b) in nitrogen.

3.4 Scanning Electron Microscopy (SEM)

A small portion of warm ABPBI dope at the end of polymerization was placed in a petri dish, which was then placed on a leveled hot plate to form uniform film. After cooled to room temperature, the dish was immersed in distilled water to let PPA diffuse out from the dope into the water to result in a coagulated, porous ABPBI film. This film was further Soxhlet-extracted with water and methanol. The SEM images of the resulting ABPBI film show that the surface texture consists of uniformly distributed fibrils (Figure 3a), indicating that high molecular weight ABPBI has been indeed obtained. Similarly, the porous films of ABPBI/SWCNT and ABPBI/MWCNT were also prepared, and their SEM images obtained from fracture surfaces are quite different from that of ABPBI. The ABPBI/SWCNT shows relatively round-shaped morphology (Figure 3c), while ABPBI/MWCNT shows relatively sharp fibril structure (Figure 3e). In both cases, the degree of CNT dispersion cannot be judged, since CNTs are well blended in ABPBI matrix and the presence of CNTs cannot be clearly discerned with SEM images.

All SEM images obtained from the fracture surfaces of sample films cast from MSA solutions (see Experimental section) display similar morphology (Figure 3b, 4d and 3f). ABPBI shows dense fibril surface (Figure 3b). Due to the diameter dimension of individual SWCNT (< 2 nm), the presence of SWCNT from the fracture surface is inconclusive by SEM at this magnification (Figure 3d). On the other hand, the fractured surface of ABPBI/MWCNT composite film shows that MWCNT is well dispersed in the ABPBI matrix (Figure 3f). Upon greater magnification, it is quite clear that the interface between ABPBI and MWCNT is not discernable (Figure 3f, inset), indicating that ABPBI and MWCNT are well bounded to each other.

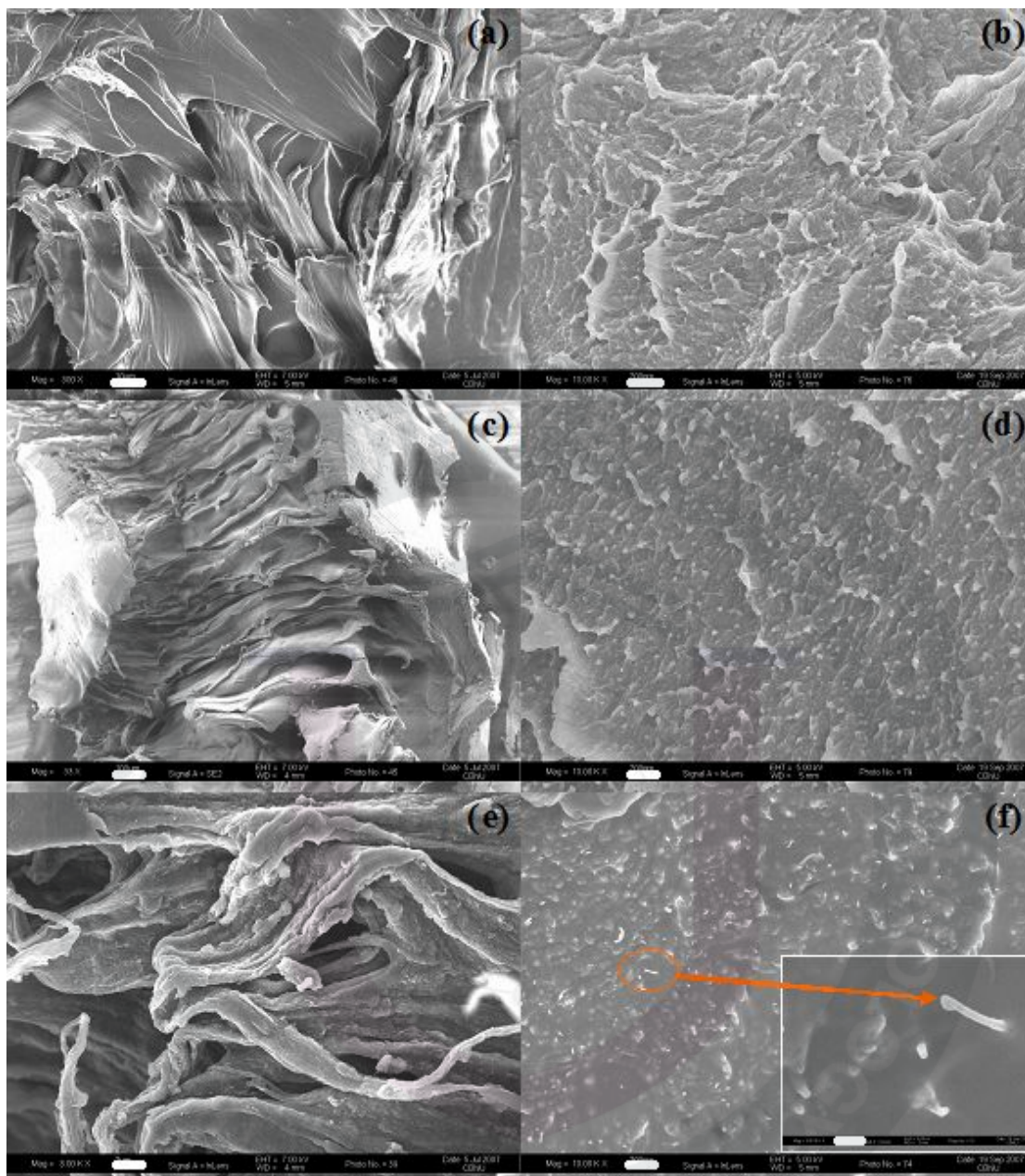


Figure 3. SEM images of samples: (a) the fracture surface of ABPBI film directly cast from reaction mixture ($\times 300$, scale bar is 20 μm); (b) the fractured surface of ABPBI film cast from MSA solution ($\times 10,000$, scale bar is 600 nm); (c) the fracture surface of ABPBI/SWCNT composite film directly cast from reaction mixture ($\times 33$, scale bar is 200 μm); (d) the fractured surface of ABPBI/SWCNT composite film cast from MSA solution ($\times 10,000$, scale bar is 600 nm); (e) the fracture surface of ABPBI/MWCNT composite film directly cast from reaction mixture ($\times 3000$, scale bar is 2 μm); and (f) the fractured surface of ABPBI/MWCNT composite film cast from MSA solution ($\times 10,000$, scale bar is 600 nm). The scale bar for the inset is 100 nm.

3.5 WAXS Patterns

To assess the dispersion quality of CNTs in ABPBI matrix, wide-angle x-ray scattering (WAXS) patterns were obtained from powder samples without applied strain. In the case of ABPBI homopolymer, two characteristic peaks at 2θ 's = 11.0 and 25.91° with respective to d -spacings = 8.03, and 3.46 Å were detected (Figure 4 and Table 2). The characteristic peak centered at about 25.91°, which corresponds to a d spacing of 3.46 Å, is the stacking of ABPBI chains.³⁴ Detected side-by-side, the inter-plane distance was slightly increased from the literature value at 3.39 to 3.41 Å because the polymer chains in powder sample was less tightly packed (Figure 4a). Interestingly, the ABPBI homopolymer prepared for this study displayed an additional strong peak that appeared at 2θ 's = 11.00° (8.03 Å). It was an indication of more ordered structure, since the sample work-up procedure was done thoroughly, and the residual reaction medium should have been completely removed (see Experimental section). On the basis of peak width and sharpness reported in the literature,³⁵ it appeared that a significant amount of residual phosphoric acid still remained in ABPBI, and it could play as an extraneous agent to disturb molecular orientation.

ABPBI/SWCNT composite displayed similar WAXS pattern to that of ABPBI (Figure 4b). The 2θ (d -spacing) values for both inter-plane π - π distance and oriented structure were slightly shifted to 10.76 (8.22 Å) and 26.01° (3.42 Å), respectively. In the case of ABPBI/MWCNT composite, a typical 2θ (d -spacing) from inter-plane π - π distance attributed to both ABPBI and MWCNT was 25.72° (3.46 Å), which was shifted by 0.19° (0.01 Å) as compared to that from ABPBI homopolymer (Figure 4c). The two peaks appeared from ABPBI homopolymer at 9.05° (9.77 Å) and 20.85° (4.26 Å) had merged into a single peak at 13.9° (6.36 Å). The metal of XRD peaks at 43.87° (2.06 Å), which would be attributed to the detachment of carbonaceous impurities and metallic particles from the SWCNT walls.

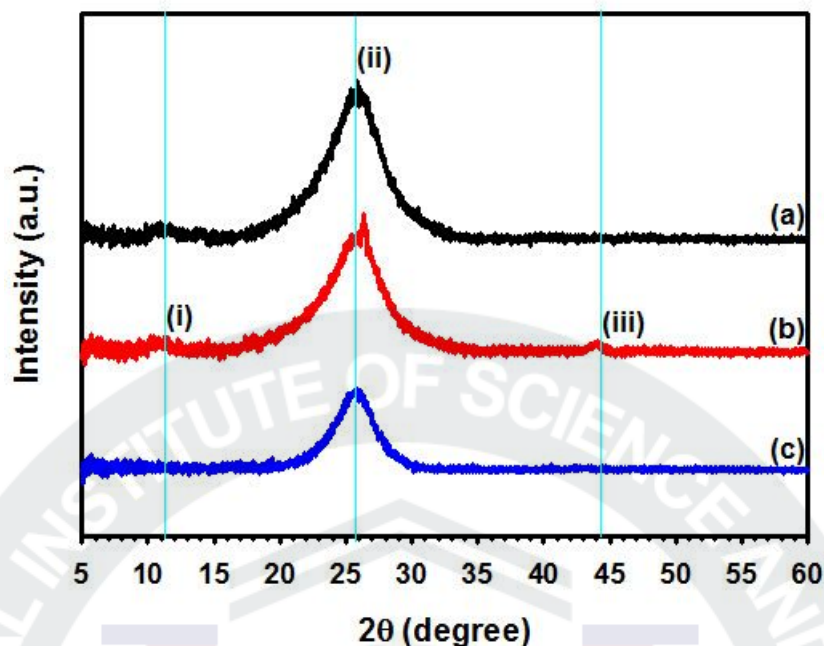


Figure 4. XRD patterns of samples: (a) ABPBI; (b) ABPBI/SWCNT; and (c) ABPBI/MWCNT.

Table 2. XRD Analysis Data of Film Samples

Sample	i		ii		iii	
	2θ (°)	<i>d</i> -Spacing (Å)	2θ (°)	<i>d</i> -Spacing (Å)	2θ (°)	<i>d</i> -Spacing (Å)
ABPBI	11.00	8.03	25.91	3.46	-	-
ABPBI/SWCNT	10.76	8.22	26.01	3.42	43.87	2.06
ABPBI/MWCNT	-	-	25.72	3.46	-	-

3.6 UV-Absorption and Emission Spectra

The photograph shown in Figure 5a is a visual demonstration as an additional support for our claim of the homogeneous dispersion of CNTs in ABPBI matrix. The ABPBI, ABPBI/SWCNT, and ABPBI/MWCNT samples were completely soluble in MSA (no CNT agglomerates visually detectable in the composite samples). They emitted strong blue light when exposed to a UV light (365 nm) from a hand-held lamp from approximately 1 foot away (Figure 5a, i-iii). The composite solutions were homogeneous and optically clear, while MWCNT and SWCNT solutions contained CNT agglomerates that were easily seen by a naked eye (Figure 5a, iv and v). To further substantiate the homogeneous dispersion of CNTs in the composite samples, UV-absorption curves were obtained from their basic solutions in *N*-methyl-2-pyrrolidinone (NMP). Since ABPBI is only soluble in strong

acids such as sulfuric acid, MSA and trifluoromethanesulfonic acid (TFMSA), UV-absorption was measured by adding a drop of MSA into its NMP solution. The absorption spectrum of protonated ABPBI consists of a strong band at 415 nm with a shoulder at 382 nm (Figure 5b). ABPBI/SWCNT and ABPBI/MWCNT composites display very similar spectra, indicating that the ground state band structure of ABPBI in composites is almost identical as that of a free ABPBI.

The emission spectra of the ABPBI and its CNT composite solutions were given in Figure 5c. The maximum emission wavelength (λ_{\max}) of ABPBI was 518 nm. In the case of composites, the emission spectra with different intensities, which were dependent on the concentration of ABPBI, were almost identical to that of neat ABPBI, implying that the excited state properties of ABPBI in the presence of CNT is also more or less unaffected. Overall, these results may also be taken as a support for our belief that the dispersion of CNTs is uniform in ABPBI matrix.

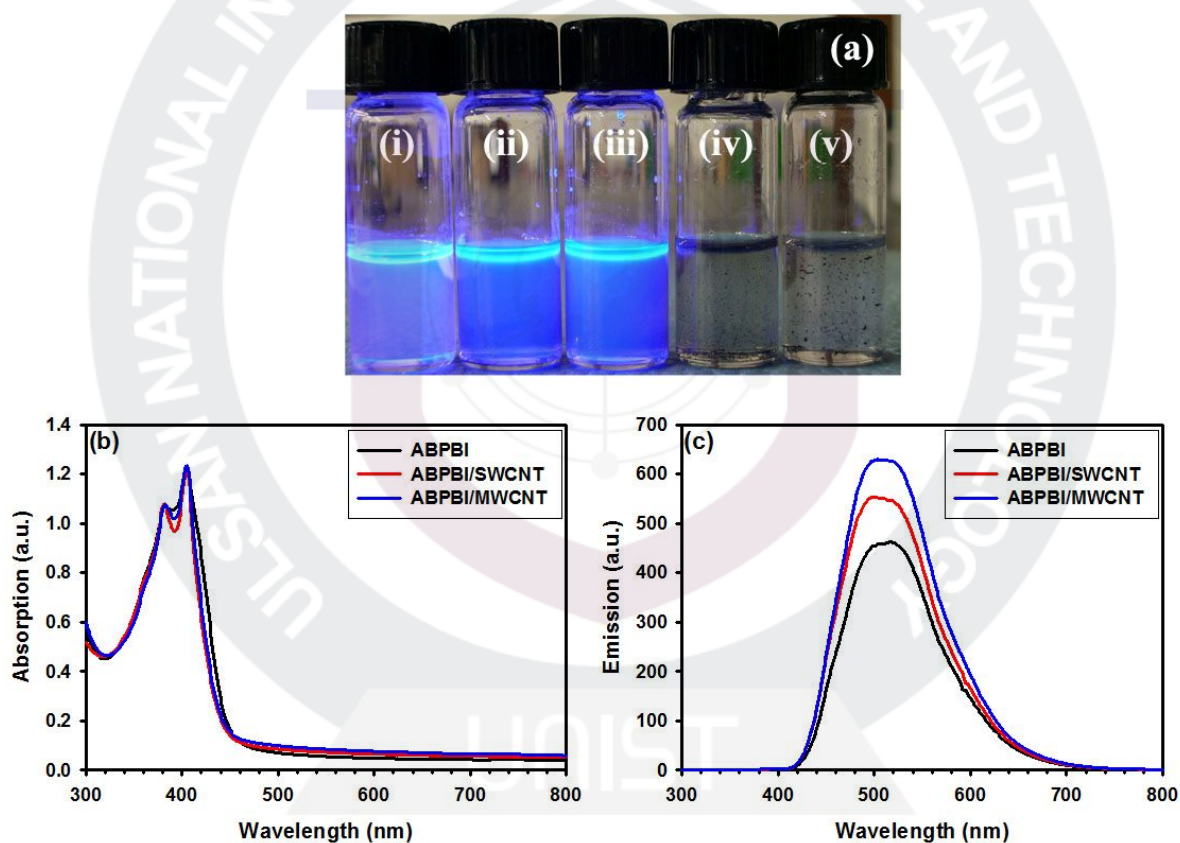


Figure 5. (a) Digital photograph of sample solutions in MSA under 365 nm UV light; (b) UV-absorption spectra of samples in NMP with a drop of MSA; and (c) emission spectra of samples in NMP with a drop of MSA. Excitation wavelength was 415 nm: (i) ABPBI; (ii) ABPBI/SWCNT; (iii) ABPBI/MWCNT; (vi) SWCNT; and (v) MWCNT.

3.7 Mechanical Properties

Cast films were cast from MSA solution and cut into specimens with size 5×70 mm and thickness 0.35-0.45 mm. Representative stress-strain curves of samples are presented in Figure 6 and the data are summarized in Table 3. The tensile strength, modulus, elongation and toughness of ABPBI film were 25 MPa, 0.88 GPa, 490% and 101.0 MPa, respectively. These values are very much different from the semi-rigid PBI prepared from AA+BB polymerization.³⁶ Specifically, elongation value was increased by almost one order of magnitude compared to the literature value.³⁶ The result could be due to the much higher molecular weight ($[\eta] = 5.23 \text{ dL/g}$) and polymer-bounded water in ABPBI. Although the former would mainly contribute to high strain-to-break value, but the influence of trapped moisture (plasticizing effect) could not be excluded. Tensile test results are generally quite subjective to the sample conditions, and therefore, the amount of bound water in the hygroscopic ABPBI sample could be another significant factor for the tensile properties measured, since the bound water can act as a plasticizer making ABPBI softer. The amount of trapped moisture can be determined by TGA. Although the residual water could be removed at elevated temperatures with/without applying vacuum, it is known that atmospheric moisture could be easily absorbed by hygroscopic ABPBI during sample preparation. Hence, all films were cast and dried at the same conditions so that the test results could be reasonable for meaningful comparison. Relative to ABPBI film, the tensile strengths of ABPBI/SWCNT and ABPBI/MWCNT composite films were significantly increased by as much as 60 and 84%, respectively. The tensile moduli of the composite films were also improved by as much as 61 and 74%, respectively. The elongation values of ABPBI/SWCNT and ABPBI/MWCNT were improved by 61 and 25%, respectively. Toughness was calculated from the area under the stress-strain curve. The ABPBI/SWCNT and ABPBI/MWCNT films had the average toughness of 210 and 200 MPa, respectively, which were increased by 108 and 98% as compared to that of ABPBI film (101 MPa). Although film and fiber properties could not be directly compared, the values are close to the nature's toughest spider silk (~215 MPa).³⁷ Thus, this notable improvement of tensile properties could be attributable to not only the higher molecular weight of ABPBI attained in this work, but also the strong interactions between ABPBI and CNT (see SEM images in Figure 3).

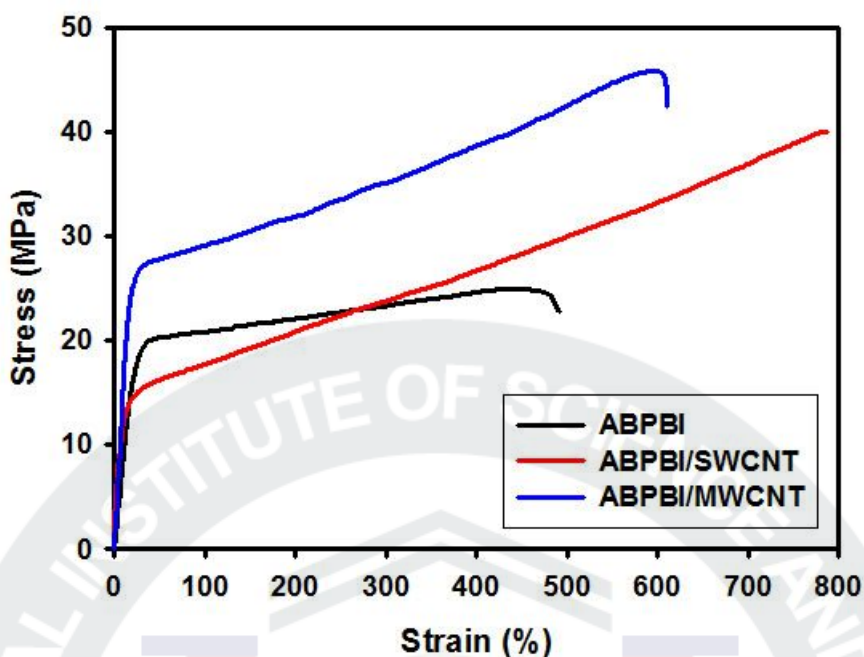


Figure 6. Representative stress–strain curves of samples, which were tested at 20 °C and relative humidity of 50%. The crosshead speed was 100% of gauge length per minute.

Table 3. Tensile Properties and Electrical Conductivity of Film Samples

Sample	Tensile Properties ^a				Electrical ^b conductivity (S/cm)
	Strength (MPa)	Modulus (Gpa)	Strain (%)	Toughness (MPa)	
ABPBI	25 ± 2	0.88 ± 0.1	490 ± 44	101.0 ± 13.8	4.81 × 10 ⁻⁶ ± 8.6 × 10 ⁻⁷
ABPBI/SWCNT	40 ± 3	1.42 ± 0.2	788 ± 80	210.0 ± 23.0	9.10 × 10 ⁻⁵ ± 8.0 × 10 ⁻⁶
ABPBI/MWCNT	46 ± 4	1.53 ± 0.2	611 ± 58	200.0 ± 19.6	2.53 × 10 ⁻¹ ± 1.0 × 10 ⁻²

^a Tensile properties were averaged values of five tests out of seven samples after the best and worst tests were discarded. Toughness was calculated from the area under the stress–strain curve in tensile test. Samples are tested at 20 °C with 50% relative humidity. The crosshead speed was 100% of gauge length per minute.

^b Electrical conductivity is an average value of 20 measurements at 20 °C with 50% relative humidity.

3.8 Electrical Conductivity of Films

The dc electrical conductivity of ABPBI homopolymer film was 4.81 × 10⁻⁶ S/cm, which was close to being an insulating material (Table 3). The ABPBI/SWCNT and ABPBI/MWCNT composite films showed 9.10 × 10⁻⁵ and 2.53 × 10⁻¹ S/cm, respectively. ABPBI/SWCNT composite film was

expected to display the better electrical conductivity, since SWCNT has the higher aspect ratio. Surprisingly, it was several orders of magnitude lower than that of ABPBI/MWCNT, which was in the semiconducting region. The higher electrical conductivity of ABPBI/MWCNT could be because of following reasons: (1) SWCNT bundles might not be well exfoliated into individual tubes; (2) the purity of as-received SWCNT was only 30-40 wt%, and thus, the actual amount of SWCNT in the ABPBI/SWCNT composite would be much lower (approximately 3-4 wt%) after *in-situ* purification in PPA (see Figure 2a); (3) another possibility is that the template polymerization of AB monomer onto the surface of SWCNT provided higher wrapping coverage, and thus insulating it because of the comparable SWCNT radius (~ 1 nm) and coil radius of ABPBI ($\sim 2.1 - 2.7$ nm).

3.9 Proton Conductivity of Films

The proton conductivity was determined with two-point probe conductivity measurement at the relative humidity of 50% (Figure 7). For benchmarking, Nafion 115 was also evaluated under the same measuring conditions, and found to display higher proton conductivity (maximum 2.95×10^{-2} S/cm at 70 °C). However, the conductivity of Nafion 115 began to drop drastically when the temperature was raised near and above 70 °C. On the other hand, ABPBI showed an initial value of 3.75×10^{-5} S/cm at 22 °C, which gradually increased as the temperature was increased, up to 1.42×10^{-4} S/cm at 140 °C before the conductivity decay started. Expectedly, the low proton conductivity of ABPBI as compared to Nafion 115 could be explained in terms of their acidity difference. The pK_a values of Nafion 115 and ABPBI are ca. ~ 6 ³⁸ and 12.75 (for benzimidazole, but for ABPBI, pK_a value is expected to be lower because of conjugative effect in the polymer backbone),³⁹ respectively. Thus, their pK_a difference is approximately ~ 18 orders of magnitude, but the difference in their maximum proton conductivities is only two orders of magnitude. It appears that in ABPBI, there is a non-linear relationship between the acidity (at the molecular level) and proton conductivity (in the bulk state), and rather surprisingly at first, there is less temperature dependence in its proton conductivity as well. We suspect that the unique features of ABPBI, namely (i) large number of benzimidazoles per polymer chain, (ii) most of benzimidazole protons should be aligned along the ABPBI chain (see Scheme 1) may, and (iii) the extended conjugation in ABPBI chain that could induce high proton mobility via tautomerization across repeat units, may be the contributing factors. Further, since the dissociation of proton from benzimidazole is a function of temperature as opposed to the complete ionization of sulfonic group at room conditions (provided that enough water are present), it is reasonable to assume that the concentration of mobile protons in ABPBI would increase with an increase in the surrounding temperature. Still, the proton conductivity of ABPBI is too low to be used as fuel cell membrane. To improve its proton conductivity, phosphoric acid or other mineral

acids are impregnated into ABPBI matrix, which results in not only the poor mechanical properties of ABPBI membrane, but acid migration to the surface of the membrane.³⁷

The maximum proton conductivity of ABPBI/SWCNT is 0.018 S/cm. The value is slightly higher than that (0.017 S/cm) of ABPBI/MWCNT. However, the proton conductivities of ABPBI/CNT films without acid doping are improved by approximately two orders of magnitude over that of ABPBI film (see Table 3). We suspect that the relatively high proton conductivity of ABPBI/CNT composite films could be originated from the proton channels along the interface of ABPBI and CNT and/or inner channel of CNT. Although further study is necessary to prove this speculation, the ABPBI/SWCNT composite film could be a good candidate for proton conducting membranes without the need for acid impregnation.

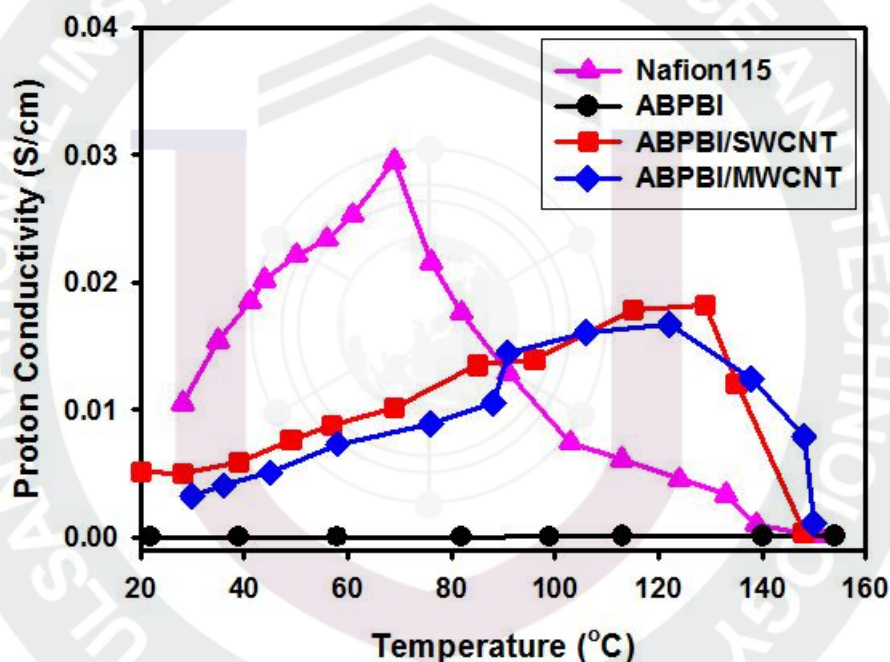


Figure 7. Proton conductivity of sample films, which was measured at relative humidity of 50%.

IV. Conclusions

Multifunctional ABPBI/CNT composites were prepared via *in-situ* polymerizations of “protonated” AB monomer. CNTs did not affect the polymerization of AB monomer to yield high molecular weight ABPBI in a mildly acidic PPA medium at 175 °C for 3h. CNTs remained structurally intact during *in-situ* polycondensation process, and under subsequent work-up conditions. It could be concluded that the reaction condition was indeed feasible for the purification (more so for SWCNT than MWCNT) and dispersion of CNTs as well as polymerization of the AB monomer in a one-pot process. The homogeneous dispersion of CNTs in ABPBI matrix was visually confirmed by

SEM imaging experiments. As a result, considerable improvement of mechanical properties of ABPBI/CNT films over ABPBI film could be achieved. Based on SEM data, we interpret that the surfaces of SWCNT and MWCNT have been decorated well with ABPBI, and since the boundary between ABPBI and CNT phases could not be discernable, homogeneous CNT dispersion in the ABPBI matrix has been achieved. Thus, load transfer from ABPBI to CNT should be efficient to result in the enhanced mechanical properties of composite films, especially the toughness. Amongst these films, ABPBI/MWCNT displayed the best electrical conductivity. ABPBI/CNT composites also showed proton conductivities without acid impregnation. Thus, electrically conducting, proton conducting, thermally stable and tough multifunctional materials were prepared. Subject to further improvement, they are potentially useful for various applications for areas, where require affordable, lightweight and high performance materials.



References

1. KELLER, T. 2001. Recent all-composite and hybrid fibre-reinforced polymer bridges and buildings. *Progress in Structural Engineering and Materials*, 3, 132-140.
2. SINHA RAY, S. & OKAMOTO, M. 2003. Polymer/layered silicate nanocomposites: a review from preparation to processing. *Progress in Polymer Science*, 28, 1539-1641.
3. BALAZS, A. C., EMRICK, T. & RUSSELL, T. P. 2006. Nanoparticle polymer composites: Where two small worlds meet. *Science*, 314, 1107-1110.
4. RAMANATHAN, T., ABDALA, A. A., STANKOVICH, S., DIKIN, D. A., HERRERA-ALONSO, M., PINER, R. D., ADAMSON, D. H., SCHNIEPP, H. C., CHEN, X., RUOFF, R. S., NGUYEN, S. T., AKSAY, I. A., PRUD'HOMME, R. K. & BRINSON, L. C. 2008. Functionalized graphene sheets for polymer nanocomposites. *Nature Nanotechnology*, 3, 327-331.
5. THOSTENSON, E. T., REN, Z. & CHOU, T. W. 2001. Advances in the science and technology of carbon nanotubes and their composites: A review. *Composites Science and Technology*, 61, 1899-1912.
6. TASIS, D., TAGMATARCHIS, N., BIANCO, A. & PRATO, M. 2006. Chemistry of Carbon Nanotubes. *Chemical Reviews*, 106, 1105-1136.
7. (a) FIEDLER, B., GOJNY, F. H., WICHMANN, M. H. G., NOLTE, M. C. M. & SCHULTE, K. 2006. Fundamental aspects of nano-reinforced composites. *Composites Science and Technology*, 66, 3115-3125. (b) GAO, J., ZHAO, B., ITKIS, M. E., BEKYAROVA, E., HU, H., KRANAK, V., YU, A. & HADDON, R. C. 2006. Chemical engineering of the single-walled carbon nanotube-nylon 6 interface. *Journal of the American Chemical Society*, 128, 7492-7496. (c) LI, N., HUANG, Y., DU, F., HE, X., LIN, X., GAO, H., MA, Y., LI, F., CHEN, Y. & EKLUND, P. C. 2006. Electromagnetic Interference (EMI) Shielding of Single-Walled Carbon Nanotube Epoxy Composites. *Nano Letters*, 6, 1141-1145. (d) MONIRUZZAMAN, M. & WINEY, K. I. 2006. Polymer Nanocomposites Containing Carbon Nanotubes. *Macromolecules*, 39, 5194-5205.
8. (a) SANDLER, J., WINDLE, A. H., WERNER, P., ALTSTADT, V., ES, M. V. & SHAFFER, M. S. P. 2003. Carbon-nanofibre-reinforced poly(ether ether ketone) fibres *Journal of Materials Science*, 38, 2135-2141. (b) KUMAR, S., DOSHI, H., SRINIVASARAO, M., PARK, J. O. & SCHIRALDI, D. A. 2002. Fibers from polypropylene/nano carbon fiber composites. *Polymer*, 43, 1701-1703. (c) ZENG, J., SALTYSIAK, B., JOHNSON, W. S., SCHIRALDI, D. A. & KUMAR, S. 2004. Processing and properties of poly(methyl methacrylate)/carbon nano fiber composites. *Composites Part B: Engineering*, 35, 173-178. (d) UCHIDA, T., DANG, T., MIN, B. G., ZHANG, X. & KUMAR, S. 2005. Processing, structure, and properties of carbon nano fiber filled PBZT composite fiber. *Composites Part B: Engineering*, 36, 183-187. (e) MA, H., ZENG, J., REALFF, M. L., KUMAR, S. & SCHIRALDI, D. A. 2003. Processing, structure, and properties of fibers

- from polyester/carbon nanofiber composites. *Composites Science and Technology*, 63, 1617-1628.
- (f) KUMAR, S., DANG, T. D., ARNOLD, F. E., BHATTACHARYYA, A. R., MIN, B. G., ZHANG, X., VAIA, R. A., PARK, C., ADAMS, W. W., HAUGE, R. H., SMALLEY, R. E., RAMESH, S. & WILLIS, P. A. 2002. Synthesis, Structure, and Properties of PBO/SWNT Composites. *Macromolecules*, 35, 9039-9043.
9. SONG, Y. S. & YOUNG, J. R. 2005. Influence of dispersion states of carbon nanotubes on physical properties of epoxy nanocomposites. *Carbon*, 43, 1378-1385.
10. (a) HAGGENMUELLER, R., GOMMANS, H. H., RINZLER, A. G., FISCHER, J. E. & WINEY, K. I. 2000. Aligned single-wall carbon nanotubes in composites by melt processing methods. *Chemical Physics Letters*, 330, 219-225. (b) L. JIN, C. B. & ZHOU, O. 1998. Alignment of carbon nanotubes in a polymer matrix by mechanical stretching. *Applied Physics Letters*, 73, 1197. (c) CHEN, G. Z., SHAFFER, M. S. P., COLEBY, D., DIXON, G., ZHOU, W., FRAY, D. J. & WINDLE, A. H. 2000. Carbon Nanotube and Polypyrrole Composites: Coating and Doping. *Advanced Materials*, 12, 522-526. (d) ZHANG, W. D., SHEN, L., PHANG, I. Y. & LIU, T. 2003. Carbon Nanotubes Reinforced Nylon-6 Composite Prepared by Simple Melt-Compounding. *Macromolecules*, 37, 256-259. (e) SANDLER, J., SHAFFER, M. S. P., PRASSE, T., BAUHOFFER, W., SCHULTE, K. & WINDLE, A. H. 1999. Development of a dispersion process for carbon nanotubes in an epoxy matrix and the resulting electrical properties. *Polymer*, 40, 5967-5971. (f) PARK, C., OUNAIES, Z., WATSON, K. A., CROOKS, R. E., SMITH, J., LOWTHER, S. E., CONNELL, J. W., SIOCHI, E. J., HARRISON, J. S. & CLAIR, T. L. S. 2002. Dispersion of single wall carbon nanotubes by in situ polymerization under sonication. *Chemical Physics Letters*, 364, 303-308. (g) SHAFFER, M. S. P. & WINDLE, A. H. 1999. Fabrication and Characterization of Carbon Nanotube/Poly(vinyl alcohol) Composites. *Advanced Materials*, 11, 937-941. (h) QIAN, D., DICKEY, E. C., ANDREWS, R. & RANTELL, T. 2000. Load transfer and deformation mechanisms in carbon nanotube-polystyrene composites. *Applied Physics Letters*, 76, 2868-2870. (i) LIU, PHANG, I. Y., SHEN, L., CHOW, S. Y. & ZHANG, W.-D. 2004. Morphology and Mechanical Properties of Multiwalled Carbon Nanotubes Reinforced Nylon-6 Composites. *Macromolecules*, 37, 7214-7222. (j) ANDREWS, R., JACQUES, D., RAO, A. M., RANTELL, T., DERBYSHIRE, F., CHEN, Y., CHEN, J. & HADDON, R. C. 1999. Nanotube composite carbon fibers. *Applied Physics Letters*, 75, 1329-1331.
11. (a) BANERJEE, S. & WONG, S. S. 2002. Synthesis and Characterization of Carbon Nanotube–Nanocrystal Heterostructures. *Nano Letters*, 2, 195-200. (b) DAI, L. & MAU, A. W. H. 2001. Controlled Synthesis and Modification of Carbon Nanotubes and C: Carbon Nanostructures for Advanced Polymeric Composite Materials. *Advanced Materials*, 13, 899-913. (c) HIRSCH, A. 2002. Functionalization of Single-Walled Carbon Nanotubes. *Angewandte Chemie International Edition*, 41, 1853-1859. (d) MITCHELL, C. A., BAHR, J. L., AREPALLI, S., TOUR, J. M. &

- KRISHNAMOORTI, R. 2002. Dispersion of Functionalized Carbon Nanotubes in Polystyrene. *Macromolecules*, 35, 8825-8830. (e) SUN, Y.-P., FU, K., LIN, Y. & HUANG, W. 2002. Functionalized Carbon Nanotubes: Properties and Applications. *Accounts of Chemical Research*, 35, 1096-1104.
12. (a) HUANG, W., LIN, Y., TAYLOR, S., GAILLARD, J., RAO, A. M. & SUN, Y.-P. 2002. Sonication-Assisted Functionalization and Solubilization of Carbon Nanotubes. *Nano Letters*, 2, 231-234. (b) ZHANG, Y., SHI, Z., GU, Z. & IIJIMA, S. 2000. Structure modification of single-wall carbon nanotubes. *Carbon*, 38, 2055-2059.
13. HELLER, D. A., BARONE, P. W. & STRANO, M. S. 2005. Sonication-induced changes in chiral distribution: A complication in the use of single-walled carbon nanotube fluorescence for determining species distribution. *Carbon*, 43, 651-653.
14. (a) HU, H., ZHAO, B., ITKIS, M. E. & HADDON, R. C. 2003. Nitric Acid Purification of Single-Walled Carbon Nanotubes. *The Journal of Physical Chemistry B*, 107, 13838-13842. (b) HUMMERS, W. S. & OFFEMAN, R. E. 1958. Preparation of Graphitic Oxide. *Journal of the American Chemical Society*, 80, 1339-1339.
15. (a) WEI, C. 2006. Adhesion and reinforcement in carbon nanotube polymer composite. *Applied Physics Letters*, 88, 93108-93110. (b) BARBER, A. H., COHEN, S. R., EITAN, A., SCHADLER, L. S. & WAGNER, H. D. 2006. Fracture Transitions at a Carbon-Nanotube/Polymer Interface. *Advanced Materials*, 18, 83-87. (c) WONG, M., PARAMSOTHY, M., XU, X. J., REN, Y., LI, S. & LIAO, K. 2003. Physical interactions at carbon nanotube-polymer interface. *Polymer*, 44, 7757-7764.
16. TRAN, M. Q., CABRAL, J. T., SHAFFER, M. S. P. & BISMARCK, A. 2008. Direct Measurement of the Wetting Behavior of Individual Carbon Nanotubes by Polymer Melts: The Key to Carbon Nanotube-Polymer Composites. *Nano Letters*, 8, 2744-2750.
17. (a) OH, S.-J., LEE, H.-J., KEUM, D.-K., LEE, S.-W., WANG, D. H., PARK, S.-Y., TAN, L.-S. & BAEK, J.-B. 2006. Multiwalled carbon nanotubes and nanofibers grafted with polyetherketones in mild and viscous polymeric acid. *Polymer*, 47, 1132-1140. (b) JEONG, W. & KESSLER, M. R. 2008. Toughness Enhancement in ROMP Functionalized Carbon Nanotube/Polydicyclopentadiene Composites. *Chemistry of Materials*, 20, 7060-7068.
18. SAEED, K., PARK, S.-Y., HAIDER, S. & BAEK, J.-B. 2009. In situ Polymerization of Multi-Walled Carbon Nanotube/Nylon-6 Nanocomposites and Their Electrospun Nanofibers. *Nanoscale Research Letters*, 4, 39-46.
19. (a) BAEK, J.-B., LYONSB, C. B. & TAN, L.-S. 2004. Covalent modification of vapour-grown carbon nanofibers via direct Friedel-Crafts acylation in polyphosphoric acid. *Journal of Materials Chemistry*, 14, 2052. (b) LEE, H.-J., HAN, S.-W., KWON, Y.-D., TAN, L.-S. & BAEK, J.-B. 2008. Functionalization of multi-walled carbon nanotubes with various 4-substituted benzoic acids

- in mild polyphosphoric acid/phosphorous pentoxide. *Carbon*, 46, 1850-1859. (c) HAN, S.-W., OH, S.-J., TAN, L.-S. & BAEK, J.-B. 2008. One-pot purification and functionalization of single-walled carbon nanotubes in less-corrosive poly(phosphoric acid). *Carbon*, 46, 1841-1849.
20. (a) WOLFE, J. E. 1988. *J. E. In Encyclopedia of Polymer Science and Technology*, New York, Wiley-Interscience. (b) ADAMS, W. W., EBY, R. K. & MCLEMORE, D. E. Year. The Materials Science and Engineering of Rigid-Rod Polymers. *In: Symposium Proceedings Materials Research Society*, 1989 Pittsburgh, PA. 351-359.
21. EO, S.-M., OH, S.-J., TAN, L.-S. & BAEK, J.-B. 2008. Poly(2,5-benzoxazole)/carbon nanotube composites via in situ polymerization of 3-amino-4-hydroxybenzoic acid hydrochloride in a mild poly(phosphoric acid). *European Polymer Journal*, 44, 1603-1612.
22. <http://www.hanhwananotech.co.kr>.
23. (a) BROCK, T. & SHERRINGTON, D. C. 1992. Preparation of spherical polybenzimidazole particulates using a non-aqueous suspension methodology. *Polymer*, 33, 1773-1777. (b) CASSIDY, P. E. 1980. *Thermally Stable Polymers.*, New York, Marcel Dekker. (c) CHUNG, T. S. 1997. *Handbook of Thermoplastics*, New York, Marcel Dekker. MILFORD, J. & GEORGE, N. 1981. *Bead polymerization process for preparing polybenzimidazole*. MILFORD, J. & GEORGE, N. 1984. *Preparation of small particle polybenzimidazole*.
24. (a) AFSHARI, M., SIKKEMA, D. J., LEE, K. & BOGLE, M. 2008. High Performance Fibers Based on Rigid and Flexible Polymers *Polymer Reviews*, 48, 230 - 274 . (b) CHAE, H. G. & KUMAR, S. 2006. Rigid-rod polymeric fibers. *Journal of Applied Polymer Science*, 100, 791-802.
25. (a) ASENSIO, J. A., BORROS, S. & GOMEZ-ROMERO, P. 2004. Polymer Electrolyte Fuel Cells Based on Phosphoric Acid-Impregnated Poly(2,5-benzimidazole) Membranes. *Journal of The Electrochemical Society*, 151, A304-A310. (b) ASENSIO, J. A., BORR S, S. & G MEZ-ROMERO, P. 2003. Enhanced conductivity in polyanion-containing polybenzimidazoles. Improved materials for proton-exchange membranes and PEM fuel cells. *Electrochemistry Communications*, 5, 967-972. (c) WAINRIGHT, J. S., LITT, M. H. & SAVINELL, R. F. 2003. *Handbook of Fuel Cell*, John Wiley & Sons, Inc.
26. ASENSIO, J. A. & G MEZ-ROMERO, P. 2005. Recent Developments on proton conducting poly(2,5-benzimidazole)(ABPBI)membranes for high temperature polymer electrolyte membrane fuel cells. *Fuel Cells*, 5, 336-343.
27. IMAI, Y., UNO, K. & IWAKURA, Y. 1965. Polybenzazoles. *Die Makromolekulare Chemie*, 83, 179-187.
28. ASENSIO, J. A., BORR S, S. & G MEZ-ROMERO, P. 2002. Proton-conducting polymers based on benzimidazoles and sulfonated benzimidazoles. *Journal of Polymer Science Part A: Polymer Chemistry*, 40, 3703-3710.

29. LITT, M., AMERI, R., WANG, Y., SAVINELL, R. & WAINWRIGHT, J. Year. Polybenzimidazoles/phosphoric acid solid polymer electrolytes: mechanical and electrical properties. *In*, 1999. 313-323.
30. KIM, H.-J., CHO, S. Y., AN, S. J., EUN, Y. C., KIM, J.-Y., YOON, H.-K., KWEON, H.-J. & YEW, K. H. 2004. Synthesis of Poly(2,5-benzimidazole) for Use as a Fuel-Cell Membrane. *Macromolecular Rapid Communications*, 25, 894-897.
31. STRANO, M. S., HUFFMAN, C. B., MOORE, V. C., O'CONNELL, M. J., HAROZ, E. H., HUBBARD, J., MILLER, M., RIALON, K., KITTRELL, C., RAMESH, S., HAUGE, R. H. & SMALLEY, R. E. 2003. Reversible, Band-Gap-Selective Protonation of Single-Walled Carbon Nanotubes in Solution. *The Journal of Physical Chemistry B*, 107, 6979-6985.
32. CHENG, J., ZHANG, X., LUO, Z., LIU, F., YE, Y. & YIN, W. 2006. Excited state proton transfer in the S1 state of 2-allylphenol, 2-propenylphenol, and 2-propylphenol and their van der Waals clusters with water and ammonia. *Mater Chem Phys* 95, 3290-3301.
33. ITKIS, M. E., PEREA, D. E., JUNG, R., NIYOGI, S. & HADDON, R. C. 2005. Comparison of Analytical Techniques for Purity Evaluation of Single-Walled Carbon Nanotubes. *Journal of the American Chemical Society*, 127, 3439-3448.
34. JR., A. W., GEHATIA, M. T. & WIFF, D. R. 1978. Morphological and physical property effects for solvent cast films of poly-2, 5(6) benzimidazole. *Polymer Engineering & Science*, 18, 204-209.
35. ASENSIO, J. A., BORR S, S. & G MEZ-ROMERO, P. 2004. Proton-conducting membranes based on poly(2,5-benzimidazole) (ABPBI) and phosphoric acid prepared by direct acid casting. *Journal of Membrane Science*, 241, 89-93.
36. KIM, T.-H., LIM, T.-W. & LEE, J.-C. 2007. High-temperature fuel cell membranes based on mechanically stable para-ordered polybenzimidazole prepared by direct casting. *Journal of Power Sources*, 172, 172-179.
37. VOLLRATH, F. & KNIGHT, D. P. 2001. Liquid crystalline spinning of spider silk. *Nature*, 410, 541-548.
38. (a) RYDER, A. G. P., SARAH; GLYNN, THOMAS J. 2003. Evaluation of Acridine in Nafion as a Fluorescence-Lifetime-Based pH Sensor *Applied Spectroscopy*, 57, 73-79. (b) KREUER, K. D. 2001. On the development of proton conducting polymer membranes for hydrogen and methanol fuel cells. *Journal of Membrane Science*, 185, 29-39.
39. CATALAN, J., CLARAMUNT, R. M., ELGUERO, J., LAYNEZ, J., MENENDEZ, M., ANVIA, F., QUIAN, J. H., TAAGEPERA, M. & TAFT, R. W. 1988. Basicity and acidity of azoles: the annelation effect in azoles. *Journal of the American Chemical Society*, 110, 4105-4111.

Appendix

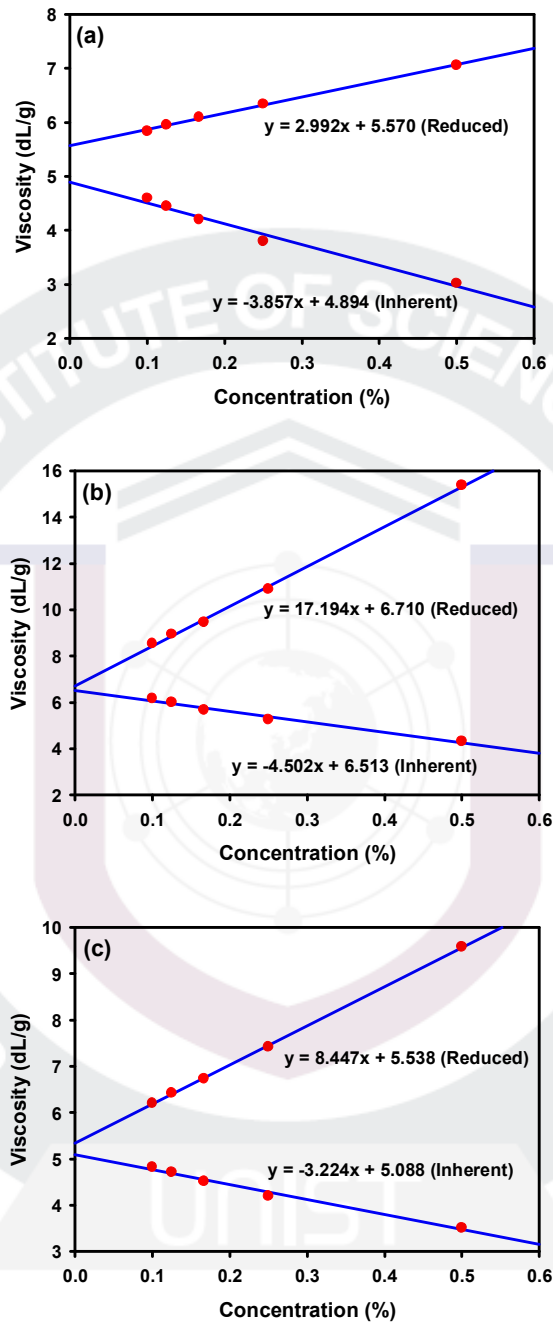


Figure S1. Solution viscosity behaviors of samples as a function of concentration in MSA: (a) ABPBI; (b) ABPBI/SWCNT; (c) ABPBI/MWCNT.

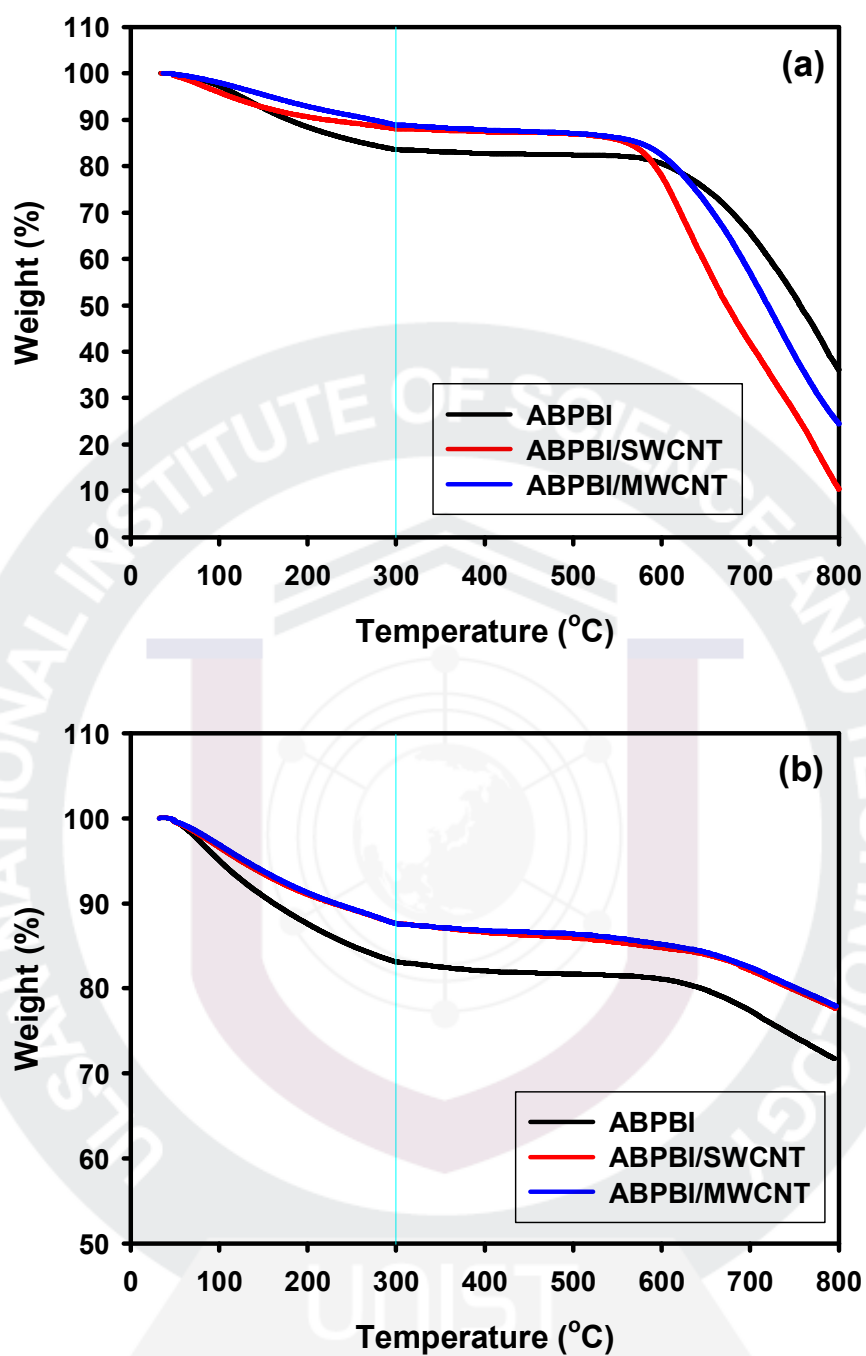


Figure S2. TGA thermograms of as-prepared sample films.

To obtain the amount of moisture in the samples, TGA analysis of ABPBI, ABPBI/SWCNT and ABPBI/MWCNT films were conducted (Figure S2). The results are summarized in Table S1. The amount of bounded water in the ABPBI film, which was determined on the basis of residual weight at 300 °C in air, was 16.4 wt%. Those of

ABPBI/SWCNT and ABPBI/MWCNT films were 11.9 and 11.1 wt%, respectively. The result implied the ABPBI/CNT composite films became less hygroscopic after incorporation of CNT. Similarly, the results obtained under nitrogen atmosphere displayed similar trend, reassuring hygroscopic behaviors of the sample films.

The sample films were further heated to 800 °C with ramping rate of 10 °C/min under air atmosphere during TGA data collection (Figure S2). The char yields of ABPBI, ABPBI/SWCNT and ABPBI/MWCNT at 800 °C in air were 36.0, 10.3 and 24.4 wt%, respectively. The results were agreed well with heat TGA results of treated samples (see Figure 3a). Again, the least char yield of ABPBI/SWCNT indicated that SWCNT was purified during polycondensation. Hence, we could conclude that PPA is an efficient medium to remove the undesired carbonaceous impurities (i.e. unstable carbonaceous fragments and amorphous carbons; see XRD discussion below) as well as catalytic residues (Ni, Fe, Co, and etc). The residual amounts of ABPBI, ABPBI/SWCNT and ABPBI/MWCNT at 800 °C in nitrogen were 72.0, 77.9 and 77.6 wt%, respectively. Not like in air, ABPBI/CNT composite films displayed the higher char yields in nitrogen, indicating that ABPBI had better thermo-oxidative stability than CNT in air.

Table S1. TGA analysis of ABPBI, ABPBI/SWCNT and ABPBI/MWCNT films

Sample	Residue at 300 °C		Char yield at 800 °C	
	In Air (%)	In N ₂ (%)	In Air (%)	In N ₂ (%)
ABPBI	83.6	83.1	36.0	72.0
ABPBI/SWCNT	88.1	87.6	10.3	77.9
ABPBI/MWCNT	88.9	87.6	24.4	77.6

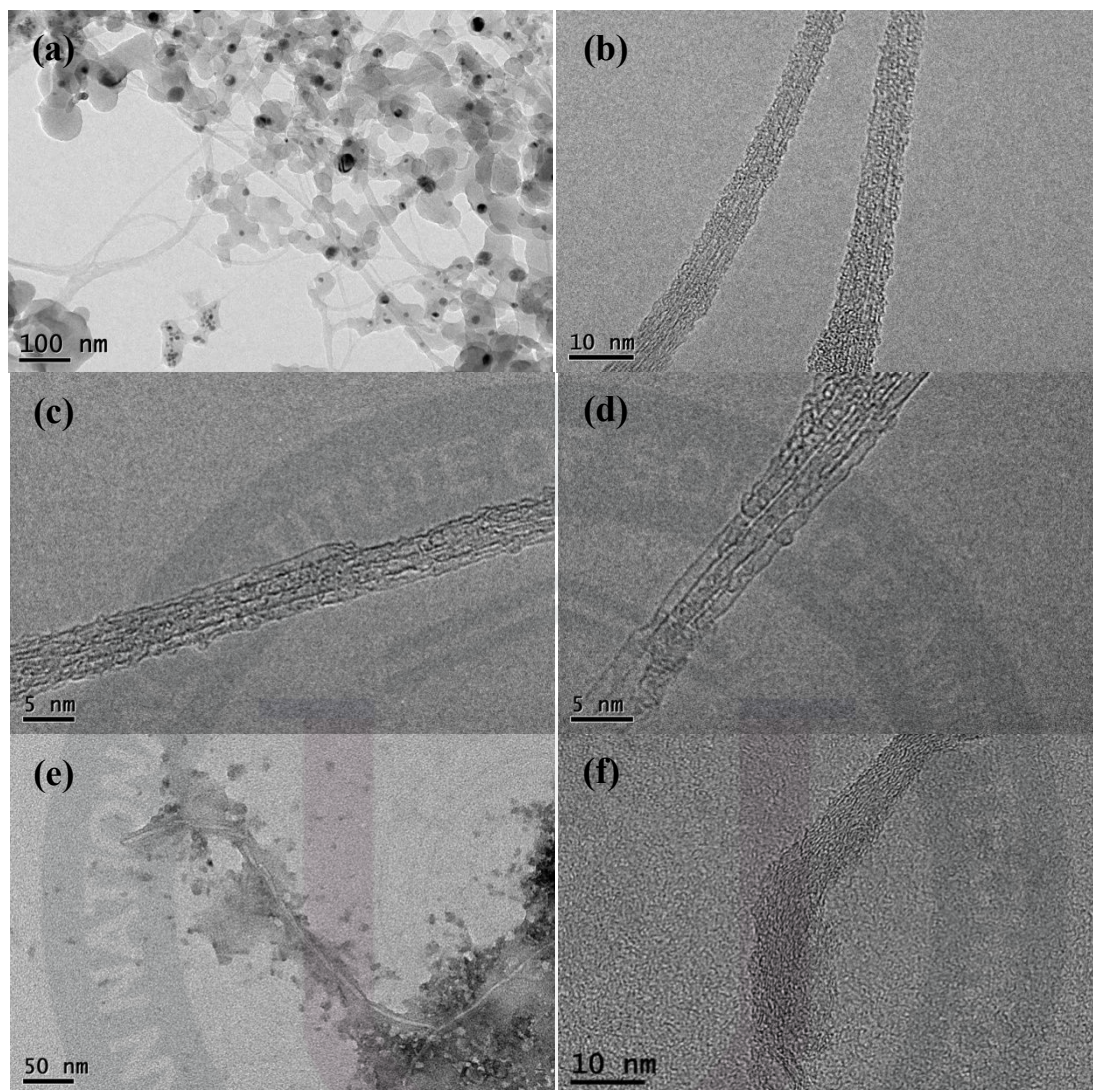


Figure S3. TEM images: (a) pristine SWCNT; (b) ABPBI/SWCNT; (c) ABPBI/SWCNT; (d) ABPBI/SWCNT; (e) ABPBI/MWCNT; (f) ABPBI/MWCNT.

For the FE-TEM analysis, ABPBI/CNT samples were dissolved in MSA. A drop of each solution was added into 10 mL NMP and the solution was drop-coated on TEM grid. The TEM image of the as-received SWCNTs shows that there are large portions of carbonaceous and metallic impurities (Figure S3a). On the other hand, the samples ABPBI/SWCNT shows that most of those impurities were removed (Figure S3b-d). The TEM images display clear stripes, which are related to crystalline structure of SWCNT, indicating that the stable crystalline carbon species are survived in the medium. Thus, it is fair to say that the PPA used in this study for the purification of SWCNT and polymerization of AB monomer selectively destroys the amorphous carbons and metallic impurities. Unlike SWCNTs that have

undergone hydrochloric acid and nitric acid/sulfuric acid treatments, there were no broken SWCNTs in bundles observed here. On the basis of these observations, PPA with or without additional P_2O_5 is indeed a mild and arguably non-destructive medium for the purification of as-received SWCNTs, and thus, SWCNTs could preserve their structural integrity, at least in a better extent than with regular acid-based purification procedures. Actually, sidewall openings could be present without being seen in TEM. In addition, ABPBI is well coated on the surface of SWCNT. For example, ABPBI is coated onto the surface of SWCNT bundle (Figure S3b), two SWCNTs (Figure S3c) and single SWCNT (Figure S3d). The images implicated that ABPBI and SWCNT are well interacted each other. Both components are conjugated structures to have strong lateral π - π interaction.

In the case of ABPBI/MWCNT sample (Figure S3e and S3f), ABPBI is coated on the surface of individual MWCNT. The concentric hollow of MWCNT can be clearly seen, but the interface between ABPBI and MWCNT cannot be clearly discerned due to the similar electron density of ABPBI and MWCNT.

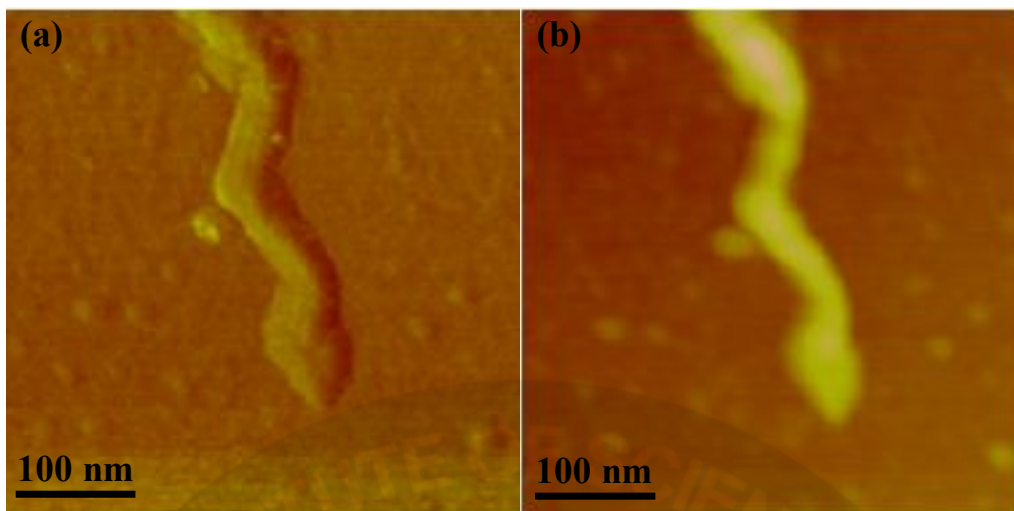


Figure S4. AFM images of ABPBI/SWCNT film cast on silicon wafer: (a) topological image; (b) height image.

AFM image obtained after ABPBI/SWCNT was dissolved in MSA. A drop of the solution was added into 10 mL NMP and the solution was spin cast on silicon wafer. The image was obtained from tapping mode, showing that the diameter of ABPBI/SWCNT is approximately 50 nm (Figure S4). On the basis of the diameter dimension of individual SWCNT (0.7-3.0 nm), ABPBI should be coated on the surface of SWCNT bundle instead of individual tube. Otherwise, the thickness of ABPBI coat onto the surface of individual SWCNT must be 24-25 nm at each side. Since the shape of tube alignment is zigzag, the template polymerization of ABPBI on the surface of individual SWCNT can be conceived (see Figure S5). In this case, ABPBI wrapped SWCNT could form bundles. Further detailed study has to be done before concluding the polymerization pattern on the surface of SWCNT.

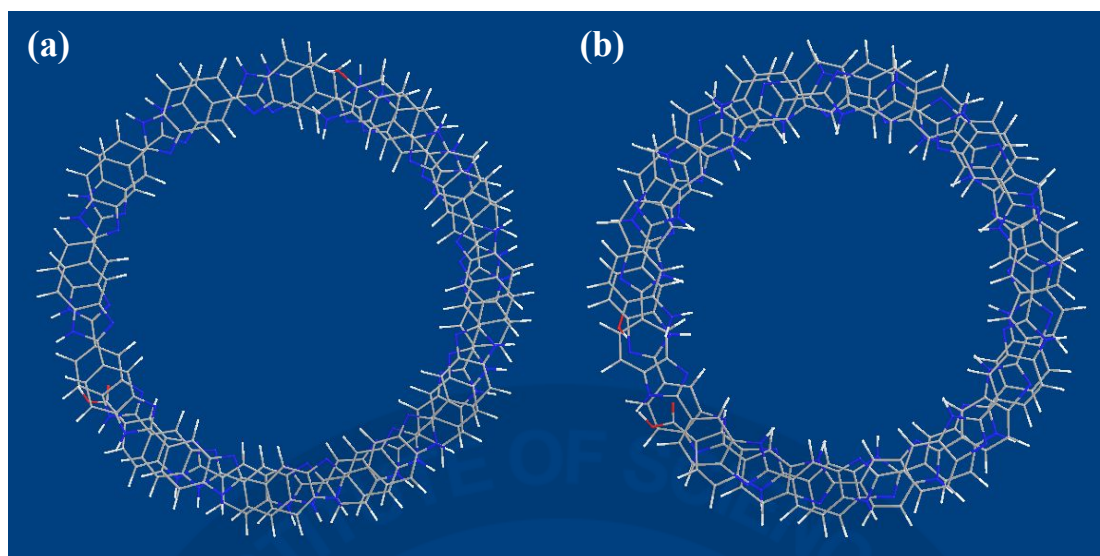


Figure S5. Structures of ABPBI coil after energy minimization with 30 repeating units: (a) *cis*-ABPBO coil; (b) *trans*-ABPBO coil shows. Both cases have interplaner π - π distance of 0.34 nm and inner diameter of *cis*-ABPBI is slightly larger than that of *trans*-ABPBI.

When ABPBI is complete *cis*-conformation, it forms well-defined coils with 12 repeating units in a period. The inner and outer diameters of the coil are approximately 21.0 (2.10 nm) and 26.6 Å (2.66 nm), respectively (Figure S5a). When ABPBI is complete *trans*-conformation, it also forms coils with 11 repeating units in a period. The inner and outer diameters of the coil are approximately 19.3 (1.93 nm) and 24.4 Å (2.44 nm) (Figure S5b), respectively, which are slightly less than its *cis*-form (Figure S5a). Interestingly, the inner diameter dimension of ABPBI is well accord with the outer diameter dimension of SWCNT (see Figure S3 in Supplementary Information). As preformed helical starch molecules could wrap SWCNT and disperse into individual tube, SWCNT could potentially be a template for the synthesis of helical *cis*- and *trans*-ABPBI depending upon diameter dimension. Thus, the complete exfoliation of SWCNT bundles into individual SWCNT is currently being investigated.

Manuscript

Paper

"Multifunctional poly(2,5-benzimidazole)/carbon nanotube composite films" J. Polym. Sci., Part A: Polym. Chem. 2010, 48, 1067 - 1078

Proceeding

International "Synthesis and Characterization of poly(2,5-benzimidazole) (ABPBI) Grafted Carbon Nanotubes." MRS. 2009 fall meeting, Prepr. Boston, MA, November 30-December 4.

"Functionalization of 3,4-diaminobenzoic acid onto the surface of carbon nanotube in polyphosphoric acid/phosphorus pentoxide medium" Polym. Prepr. 2009, 49(2), Salt Lake, UT, March 22-26.

"Synthesis and characterization of poly(2,5-benzimidazole) (ABPBI) grafted carbon nanotube" The polymer Society of Korea 2010, 35(1), (Daejeon, April 8-9).

"Functionalization of 3,4-diaminobenzoic acid into the surface of Carbon nanotubes in Polyphosphoric acid/Phosphorous Pentoxide medium" The polymer Society of Korea 2009, 34(2), (Gwangju, October 8-9).

Domestic "Preparation and Characterization of PVA/MWNT and PVA/HB-MWNT Composite Films" The Polymer Society of Korea 2009, 34(1) (Daejeon, April 9-10).

"Functionalization of 3,4-Diaminobenzoic Acid onto the Surface of Carbon Nanotube in Polyphosphoric acid/Phosphorous Pentoxide Medium" The Polymer Society of Korea 2008, 33(2). (KINTEX, ILSAN, October 9-10, 2008).

"Template Synthesis of Poly(2, 5-benzimidazole) in the Presence of Carbon Nanotubes" The Polymer Society of Korea 2008, 33(1) (Daejeon, April 11-12).

Acknowledgment

First of all, I want to thank my parents for believe me. When I had to confront a critical decision about moving graduate school, you supported my decision. I'll remember your mention about that you have to become a man who is true to your name and not a woman. And I always tank you, my sister. You always listen to my concern as like friend.

My advisor gave me suggestion whenever I ask for it and he advised me on what to do first. I think I owe what I am to my professor Jong-Beom Baek. I'm wholeheartedly thankful for his advice. I'd like to thank you to all member of laboratory. None of this result would have been possible without your help.

I feel so relieved that the defense is over. It's going to be a whole new challenge after graduate. Please keep your fingers crossed for me.

